Report No. KS-24-03 ▪ FINAL REPORT ▪ July 2024

Field Monitoring of a Mechanically Stabilized Earth Wall Backfilled with Lightweight Cellular Concrete

Robert L. Parsons, Ph.D., P.E.
Hao Liu, Ph.D.
Jie Han, Ph.D., P.E.

The University of Kansas

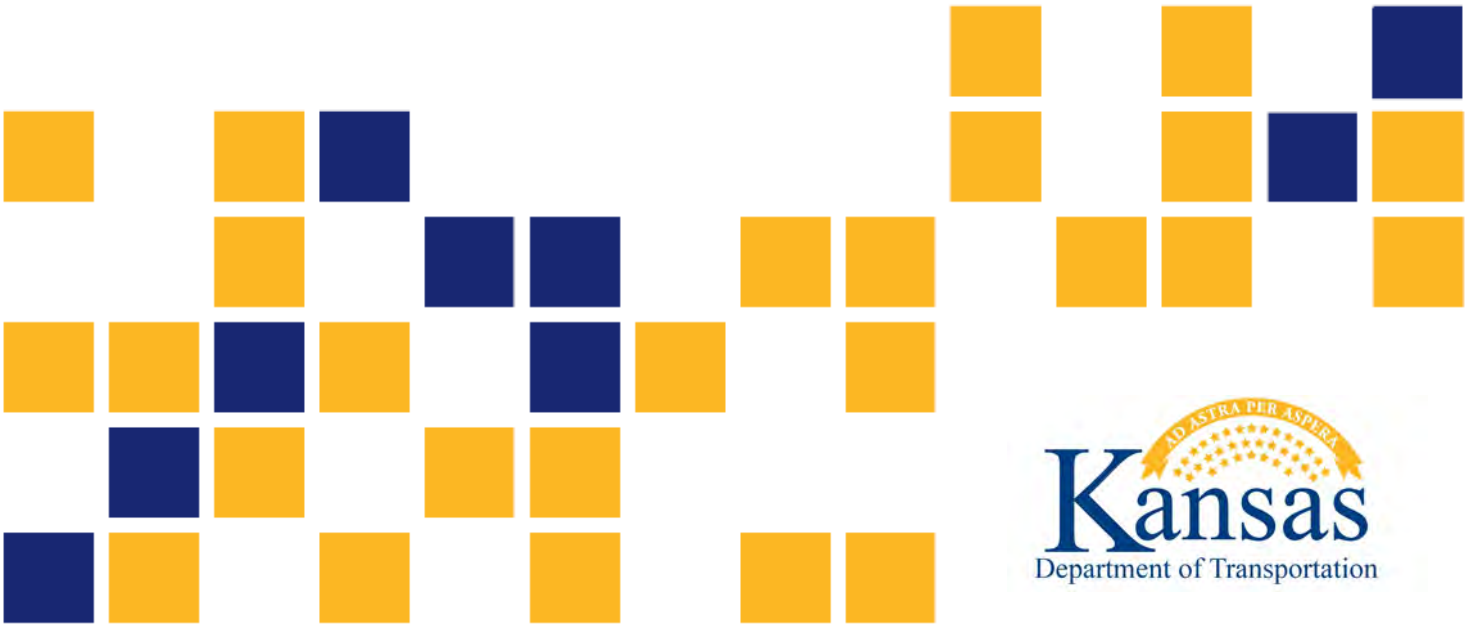

Kansas
Department of Transportation

1 Report No. KS-24-03	**2 Government Accession No.**	**3 Recipient Catalog No.**
4 Title and Subtitle Field Monitoring of a Mechanically Stabilized Earth Wall Backfilled with Lightweight Cellular Concrete		**5 Report Date** July 2024 **6 Performing Organization Code**
7 Author(s) Robert L. Parsons, Ph.D., P.E., Hao Liu, Ph.D., Jie Han, Ph.D., P.E.		**8 Performing Organization Report No.**
9 Performing Organization Name and Address The University of Kansas Department of Civil, Environmental & Architectural Engineering 1530 West 15th St Lawrence, Kansas 66045-7609		**10 Work Unit No. (TRAIS)** **11 Contract or Grant No.** C2158
12 Sponsoring Agency Name and Address Kansas Department of Transportation Bureau of Research 2300 SW Van Buren Topeka, Kansas 66611-1195		**13 Type of Report and Period Covered** Final Report April 2020 – June 2022 **14 Sponsoring Agency Code** RE-0819-01
15 Supplementary Notes For more information write to address in block 9.		

16 Abstract

As an alternative to aggregate as backfill material in mechanically stabilized earth (MSE) walls, lightweight cellular concrete (LCC) significantly reduces the weight of MSE wall mass, corresponding settlement of the foundation soil, and lateral earth pressures behind wall facing. Steel strips, geogrids, or steel rods are commonly used to reinforce the LCC in an LCC-MSE wall. This research used LCC to replace a test section with aggregate backfill in a new MSE wall on I-35 in Kansas to investigate LCC performance. Seven steel reinforcement strips of various lengths were pulled out of the backfill at different times in the curing process to study the effects of curing time and length on pull-out capacities. In addition, the LCC-MSE wall was instrumented with earth pressure cells, shape arrays, thermistors, strain gauges, and survey targets to explore LCC-MSE wall performance.

Settlements were very low under the weight of the LCC, with maximum settlement less than 0.3 inches partly due to apparent rotation of the fill mass because of horizontal pressures behind the mass. Lateral earth pressures were a function of the fluid density of the LCC during placement but dropped to near zero for most of the facing during curing. Lateral earth pressures for the top panel experienced significant fluctuations with ambient air temperatures. High temperatures exceeding 190 °F within the mass early in the curing process may complicate future designs. Reinforcement pullout strengths were much higher than reinforcement strengths in aggregate with similar normal stress. A modest reduction in pullout resistance was observed over the first 14 days, possibly due to decreased normal stress due to cooling. Overall, cement hydration increased interface strength between LCC and steel strips, thereby increasing pullout capacities of steel strips.

17 Key Words Earth Walls, Mechanically Stabilized Earth, Lightweight Concrete, Cellular Concrete, Retaining Walls		**18 Distribution Statement** No restrictions. This document is available to the public through the National Technical Information Service www.ntis.gov.	
19 Security Classification (of this report) Unclassified	**20 Security Classification (of this page)** Unclassified	**21 No. of pages** 81	**22 Price**

Form DOT F 1700.7 (8-72)

This page intentionally left blank.

Field Monitoring of a Mechanically Stabilized Earth Wall Backfilled with Lightweight Cellular Concrete

Final Report

Prepared by

Robert L. Parsons, Ph.D., P.E., F.ASCE
Hao Liu, Ph.D.
Jie Han, Ph.D., P.E., F.ASCE

The University of Kansas

A Report on Research Sponsored by

THE KANSAS DEPARTMENT OF TRANSPORTATION
TOPEKA, KANSAS

and

THE UNIVERSITY OF KANSAS
LAWRENCE, KANSAS

July 2024

NOTICE

The authors and the state of Kansas do not endorse products or manufacturers. Trade and manufacturers' names appear herein solely because they are considered essential to the object of this report.

This information is available in alternative accessible formats. To obtain an alternative format, contact the Office of Public Affairs, Kansas Department of Transportation, 700 SW Harrison, 2nd Floor – West Wing, Topeka, Kansas 66603-3745 or phone (785) 296-3585 (Voice) (TDD).

DISCLAIMER

The contents of this report reflect the views of the authors who are responsible for the facts and accuracy of the data presented herein. The contents do not necessarily reflect the views or the policies of the state of Kansas. This report does not constitute a standard, specification, or regulation.

Abstract

As an alternative to aggregate as backfill material in mechanically stabilized earth (MSE) walls, lightweight cellular concrete (LCC) significantly reduces the weight of MSE wall mass, corresponding settlement of the foundation soil, and lateral earth pressures behind wall facing. Steel strips, geogrids, or steel rods are commonly used to reinforce the LCC in an LCC-MSE wall. This research used LCC to replace a test section with aggregate backfill in a new MSE wall on I-35 in Kansas to investigate LCC performance. Seven steel reinforcement strips of various lengths were pulled out of the backfill at different times in the curing process to study the effects of curing time and length on pull-out capacities. In addition, the LCC-MSE wall was instrumented with earth pressure cells, shape arrays, thermistors, strain gauges, and survey targets to explore LCC-MSE wall performance.

Settlements were very low under the weight of the LCC, with maximum settlement less than 0.3 inches partly due to apparent rotation of the fill mass because of horizontal pressures behind the mass. Lateral earth pressures were a function of the fluid density of the LCC during placement but dropped to near zero for most of the facing during curing. Lateral earth pressures for the top panel experienced significant fluctuations with ambient air temperatures. High temperatures exceeding 190 °F within the mass early in the curing process may complicate future designs. Reinforcement pullout strengths were much higher than reinforcement strengths in aggregate with similar normal stress. A modest reduction in pullout resistance was observed over the first 14 days, possibly due to decreased normal stress due to cooling. Overall, cement hydration increased interface strength between LCC and steel strips, thereby increasing pullout capacities of steel strips.

Acknowledgements

This research project was financially sponsored by the Kansas Department of Transportation (KDOT) through the Kansas Transportation Research and New Developments (K-TRAN) program. Mr. Luke Metheny, Chief Geotechnical Engineer, KDOT Bureau of Structures & Geotechnical Services, was the monitor for this project, and Mr. James Brennan and Mr. Nathan Jeffries of KDOT provided excellent technical and field assistance. Technicians Kent Dye and David Woody from the Civil, Environmental & Architectural Engineering (CEAE) Department at the University of Kansas assisted in making and revising the field pullout device. M.S. student Cameron Dupont and Ph.D. students Yuqiu Ye, Md Wasif Zaman, and Turki Alsharari from the CEAE Department at the University of Kansas provided kind assistance during preparation and installation of the instrumentation and during field pullout tests. All the above support and assistance is greatly appreciated.

Table of Contents

Abstract v
Acknowledgements vi
Table of Contents vii
List of Tables ix
Lists of Figures ix
Chapter 1: Introduction 1
1.1 Background 1
1.2 Problem Statement 2
1.3 Research Objective 3
1.4 Research Methodology 3
1.5 Report Organization 3
Chapter 2: Project and Instrumentation 5
2.1 Project Introduction 5
2.2 Construction Stages 7
2.3 Lightweight Cellular Concrete 7
2.4 Ribbed Steel Strip Reinforcement 9
2.5 Instrumentation 11
2.6 Data Reduction 13
Chapter 3: Field Pullout Tests 17
3.1 Test Setup 17
3.2 Test Results and Analysis 19
3.2.1 Temperature Sensor Layout and Measurements for the LCC 19
3.2.2 Pullout Capacity 20
3.3 Discussion 27
3.4 Conclusions 29
Chapter 4: MSE Wall Construction and LCC Curing 30
4.1 Pressure and Temperature 30
4.2 Force and Moment of Strips 37
4.3 Lateral Deformation and Settlement 40

4.4 Conclusions 43
Chapter 5: MSE Wall Performance 45
5.1 Vertical and Lateral Earth Pressures 45
5.2 LCC and Wall Facing Settlements 56
5.3 Temperature Changes 60
5.4 Conclusions 63
Chapter 6: Conclusions and Recommendations 64
6.1 Conclusions 64
6.2 Recommendations 65
References 67

List of Tables

Table 2.1: Construction Stages of LCC-MSE Wall 7
Table 2.2: Information for Steel Strips and Pullout Tests 10

Lists of Figures

Figure 2.1: Front View of LCC-MSE Wall 6
Figure 2.2: Typical Cross Section of LCC-MSE Wall 6
Figure 2.3: Unit Weight of LCC Over Time 8
Figure 2.4: Unconfined Compressive Strength of LCC Over Time 8
Figure 2.5: Placement of the Second LCC Layer 9
Figure 2.6: Layout of Steel Strips for Field Pullout Tests (Front View) 10
Figure 2.7: Layout of Instrumentation 12
Figure 2.8: Top View of Reference Point, Total Station, and Survey Targets 13
Figure 2.9: Method for Reading Survey Targets 15
Figure 3.1: (a) Test Device; (b) Setup 18
Figure 3.2: (a) Temperature Sensor Layout; (b) Temperature Change over Time in LCC 20
Figure 3.3: Pullout Tests of Short Strips 21
Figure 3.4: Change of Peak and Residual Forces Over Time 25
Figure 3.5: Pullout Test of Long Strip (Strip #5) 27
Figure 3.6: Comparison of LCC Field Tests and Aggregate 29
Figure 4.1: Pressures during LCC Placement 30
Figure 4.2: Temperatures during LCC Placement 31
Figure 4.3: Pressures During LCC Curing 34
Figure 4.4: Temperatures During LCC Curing 35
Figure 4.5: Readouts of Strain Gauges (Strip #5) 38
Figure 4.6: Force and Moment at Front End of Strips 39
Figure 4.7: Temperature and Displacement Measured by Vertical Shape Array 41
Figure 4.8: Temperature and Settlement Measured by Horizontal Shape Array 42
Figure 5.1: Effects of PCCP Layer Placement on Vertical and Lateral Earth Pressures 46

Figure 5.2: Vertical and Lateral Earth Pressures (November 2020 to November 2021)..... 47
Figure 5.3: Variations of Vertical and Lateral Earth Pressures 49
Figure 5.4: Average Vertical and Lateral Earth Pressures..... 50
Figure 5.5: (a) Relationship between Average Vertical and Lateral Earth Pressures and (b) Air Temperature 52
Figure 5.6: Effects of Daily Air Temperature on (a) Temperatures and (b) Vertical Earth Pressures at LCC base 53
Figure 5.7: Effects of Daily Air Temperature on (a) Temperatures and (b) Lateral Earth Pressures behind Wall Facing 54
Figure 5.8: (a) Temperatures and (b) Pressures at 0:00 on July 29 and November 3, 2021..... 55
Figure 5.9: (a) Temperatures and (b) Settlements of LCC Measured by Shape Array 57
Figure 5.10: Settlements of LCC Measured by Shape Array 58
Figure 5.11: (a) Deformations and (b) Settlements of Wall Facing 59
Figure 5.12: Temperatures from November 2020 to November 2021 60
Figure 5.13: Relationship between Average Air Temperatures and Average Measured Temperatures..... 62

Chapter 1: Introduction

When used as an alternative to aggregates as backfill material, lightweight cellular concrete (LCC) can decrease the self-weight of mechanically stabilized earth (MSE) walls by 75% or more compared to aggregate backfill, leading to a corresponding reduction in ground settlements. In addition, after curing, LCC typically exerts little to no lateral earth pressure on the back of the wall facing. Therefore, LCC is an excellent substitute for MSE backfill aggregate for walls on soft ground. However, research on the performance of LCC-MSE walls and the interaction between reinforcement and LCC is limited. This report provides the results from a study of an LCC-MSE wall test section, including vertical earth pressures and settlement, lateral earth pressures, temperatures throughout the fill, and pullout resistance of reinforcement at various points in the curing process for approximately one year.

1.1 Background

When creating LCC with cast unit weights ranging from 20 to 80 pcf, prepared foam or foam agents are added to a cementitious slurry to generate gas within the slurry with or without fly ash, sand, or other material, such as lightweight aggregate (Fouad, 2006; Nambiar & Ramamurthy, 2006; Pradel & Tiwari, 2015; Taylor & Halsted, 2021). LCC strength increases as the unit weight increases, but its thermal capacity and sound insulation potential decrease (Fouad, 2006). Applications for LCC with a cast unit weight less than 50 pcf include void fill, trench reinstatement, lateral load reduction on wall structures, floor fill, and underground thermal conduit lining due to its thermal and sound insulation properties. Replacement of aggregate with LCC in MSE walls has been shown to decrease settlement of the foundation soil due to its lighter unit weight and decrease inertia load and dynamic compression in an earthquake (Pradel & Tiwari, 2015). Geosynthetics or steel strips are commonly used to stabilize backfill and hold the MSE wall facing in place. Since the unconfined compressive strength of LCC is much higher than conventional backfill material (i.e., aggregate), LCC is expected to exert minimal to no lateral earth pressure on the back of the MSE wall facing after setting.

LCC-MSE walls have been constructed in Illinois, Missouri, and California. In California, the unit weight of LCC for an MSE wall typically ranges from 19 to 37 pcf and the uniaxial compressive strength (UCS) is 73–435 psi (Pradel & Tiwari, 2015). Wall panels have been necessary for LCC-MSE walls; although, hardened LCC may not exert lateral earth pressures on the back facing of wall panels. LCC is a moderately viscous fluid during LCC placement, exerting approximately hydraulic pressures on the back facing of wall panels. Therefore, external bracing is necessary to support wall panels during LCC placement. However, hardened LCC behaves like a porous, soft rock, meaning minor vehicle impact may damage it; thereby, necessitating protection for wall panels. The wall panels for an LCC-MSE wall are typically placed in an offset-alternate pattern and anchored into the infill by layers of reinforcements (e.g., steel strip, steel rod, and geogrids) with typical spacing of 2.5 ft in both the horizontal and vertical directions. Reinforcements can be connected to wall panels by high-strength bolts through the reinforcing strips and the embedded tie strips, interlocking loops, or connecting pins. The strips are supported by rebar stakes or chairs, and the spacing of these supports along the strip length are limited to avoid strip sagging. Furthermore, reinforcement strips should be placed at least 6 inches above cold joints, if present, to avoid decreased pullout resistance. To avoid outflows of LCC through the joints between wall panels, geotextile typically is glued to the back facing of wall panels to seal these joints.

1.2 Problem Statement

The interaction between LCC and reinforcements such as steel strips must be investigated to optimize LCC-MSE wall design efficiency and performance. Many field (Chang, Chang, Yang, & Yan, 2000) and lab tests (Jayawickrama, Lawson, Wood, & Surles, 2015; Weldu et al., 2016; Rahmaninezhad, Han, & Kakrasul, 2018) have been conducted on steel strips in cohesionless backfill material. Ramezani, Vilches, and Neitzert (2013) and Sayadi, Vilches, Neitzert, and Clifton (2016a, 2016b) conducted numerical analyses and physical model tests to investigate the pullout strength of galvanized steel strips with various geometries and hole patterns encased in LCC. According to Sayadi et al. (2016a, 2016b), steel strips experienced chemical bond failure, mechanical interlocking bond failure, shear-off failure, and pullout failure when the steel strip was

pulled out from LCC. In addition, locking areas in the strip behaved as shear keys, similar to ribs on steel bars to increase the interlocking bonds. Based on lab tests of pullout capacities of geogrids and steel strips encased in LCC, Ye et al. (2022) found that pullout resistance of geogrids and steel strips increased as the age of the LCC and the fly ash ratio increased. In addition, increased normal stress improved the pullout resistance of geogrids, but not the resistance of the steel strips. However, limited results of pullout tests of steel strips encased in LCC were found by the authors in the published literature. Although LCC-MSE walls demonstrated advantages over MSE walls infilled with aggregates, limited published work of field monitoring for LCC-MSE walls was available before the time of this report.

1.3 Research Objective

The objective of this research was to investigate the suitability of using LCC as a substitute backfill material in place of aggregate. Specific subjects of the investigation included settlement, vertical and lateral earth pressures, temperatures from curing and the effect of temperature changes, interactions between LCC and steel strips via field pullout tests, and the general performance of an LCC-MSE wall via field monitoring for more than one year after its construction.

1.4 Research Methodology

A 50-ft long test section with LCC substituted for aggregate backfill was constructed and monitored for this research. Monitoring included vertical and lateral earth pressures, settlements and lateral deformation of the wall, temperatures throughout the mass, and reinforcement pullout. For the pullout testing, steel strips of various lengths and ages after LCC casting were loaded in tension until pullout failure was reached. Monitoring data was collected for slightly more than one year after construction.

1.5 Report Organization

This report consists of six chapters. Chapter 1 introduces the background, problem statement, research objective, research methodology, and report organization. Chapter 2 presents detailed information on the construction of the LCC-MSE wall, the instrumentation installed, and

methods to address field monitoring data. Chapter 3 contains an analysis of the field pullout tests for seven strips encased in LCC with regard to the impact of curing time and strip length on the pullout capacity. Chapter 4 presents field monitoring data during LCC-MSE construction and the first month after LCC-MSE construction. Chapter 5 presents an analysis of one year of field monitoring data from November 2020 to November 2021 to investigate the performance of the LCC-MSE wall over time. Chapter 6 summarizes the findings from this research and makes recommendations regarding the use of LCC for future walls.

Chapter 2: Project and Instrumentation

This chapter contains descriptions of the LCC-MSE wall components, including the LCC and steel reinforcement, and its construction stages, as well as descriptions of the instrumentation and its placement, including layouts of instrumentation for earth pressure cells, thermistors, shape arrays, and survey targets. Finally, this chapter describes the methods used to analyze the data collected from this instrumentation.

2.1 Project Introduction

To meet increasing traffic requirements near the interchange between Interstate 35 (I-35) and 75th Street in Johnson County, Kansas, an MSE wall with aggregate backfill was designed to support a shoulder and one additional lane for the existing north-bound side of I-35. A 50-ft long trial segment of this MSE wall was backfilled with LCC to study the performance of an LCC-MSE wall (Figure 2.1). The two columns shown in Figure 2.1 represent the boundaries of the LCC-MSE wall with a conventional MSE wall (i.e., AG-MSE). The wall facing of the LCC-MSE wall was comprised of six columns of 6-in. thick wall panels placed in an offset-alternate pattern, and each column was comprised of two or three panels. The widths of the first five columns (from left to right) were approximately 9 ft, while the sixth column was 5 ft wide. The horizontal spacings of the steel strips used to reinforce the LCC-MSE wall were 27 inches, while the vertical spacings were approximately 15 or 30 inches. Figure 2.2 shows a cross section of the LCC-MSE wall.

A portion of the ground in front of the designed wall facing was excavated for construction convenience, and then an unreinforced concrete leveling pad (6 in. thick and 12 in. wide) was cast in-place to support the wall panels. As shown in Figure 2.1, the vertical dimension of the bottom wall panel at the primary instrumentation location was 6.2 ft, while the vertical dimension of the top wall panel was 4.0 ft. Bearing pads with a thickness of 0.75 inches were placed on top of the bottom wall panel to support the top wall panel, and a geotextile with a width of 12 in. was glued along joints of the wall panels to prevent LCC outflow during LCC placement. The height of the LCC-MSE wall was 11.5 ft from the top of the leveling pad, including 10 ft of LCC backfill, a 4-in.-thick FA-A aggregate cushion layer, a 4-in.-thick cement-treated base (CTB) layer, and a 12-in.-thick portland cement concrete pavement (PCCP) in that order from the bottom to the top.

Five layers of 12-ft-long steel reinforcing strips were installed at elevations of 1.25, 2.50, 5.00, 7.50, and 8.75 ft from the top of leveling pad and connected with pre-cast tie tabs on the backs of the wall panels by high-strength bolts. The galvanized steel strip used in the LCC-MSE wall was 2 in. wide and 0.16 in. thick.

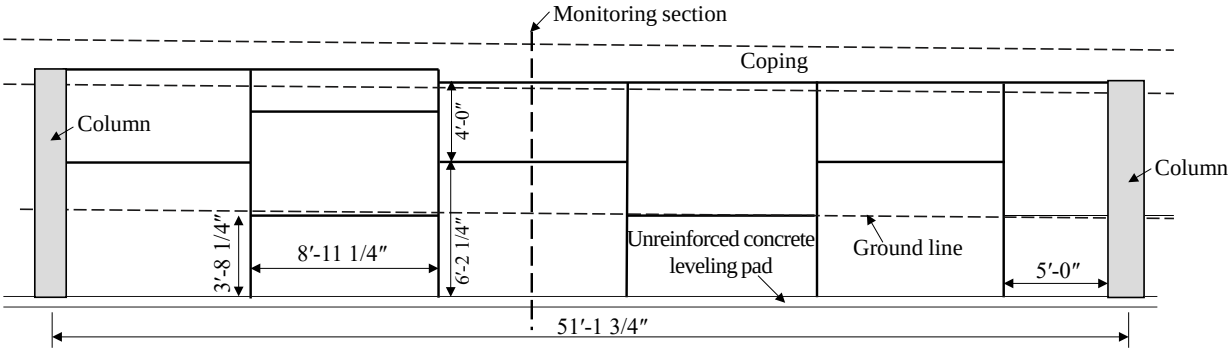

Figure 2.1: Front View of LCC-MSE Wall
Source: modified from Liu, Robert, Han, Ye, & O'Reilly (2022)

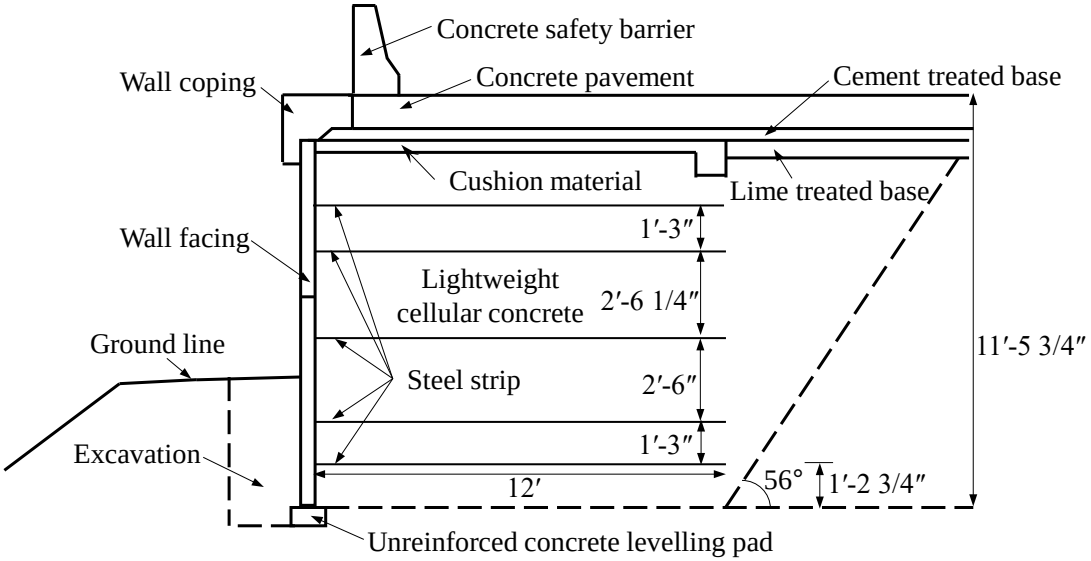

Figure 2.2: Typical Cross Section of LCC-MSE Wall
Source: modified from Liu et al. (2022)

2.2 Construction Stages

Table 2.1 shows construction stages and timelines of the LCC-MSE wall. LCC backfill was placed in four layers from September 28 to October 1, 2020. The 4-inch-thick cushion layer, 4-inch-thick CTB layer, and 12-inch-thick PCCP layer were placed on October 16, October 21 and 22, and December 2, 2020, respectively. After construction of the CTB layer, the excavated portion of the original ground in front of the wall facing was backfilled on October 29, 2020, before placing the PCCP layer on December 2, 2020.

Table 2.1: Construction Stages of LCC-MSE Wall

Stage	Construction stages	Date and time	Elevation of top surface (ft)
1	First LCC layer	September 28, 2020, 13:20–15:40	2.9
2	Second LCC layer	September 29, 2020, 13:00–14:00	5.8
3	Top panel and third LCC layer	September 30, 2020, 14:40–15:40	8.3
4	Fourth LCC layer	October 1, 2020, 14:20–15:00	10.0
5	Coping	October 12–14, 2020	10.0
6	Cushion layer	October 16, 2020	10.2
7	Cement-treated base (CTB)	October 21–22, 2020	10.5
8	Backfill soil in front of wall facing	October 29, 2020	10.5
9	Portland cement concrete pavement (PCCP)	December 2, 2020	11.5

Note: Elevation of the top surface was from the top of the leveling pad.

2.3 Lightweight Cellular Concrete

The LCC used for this project was a mixture of cement, fly ash, water, and foam. The contents of cement and fly ash in the LCC were 75% and 25% by weight, respectively. The cast unit weight of LCC was approximately 30 pcf. Cylinder samples with a height of 6 in. and diameter of 3 in. were cast on site and cured in a moisture room for lab testing. Figure 2.3 shows the dry and wet unit weights of LCC on different days after LCC casting. Dry and wet unit weights increased from 24 pcf to 27 pcf and from 33 pcf to 42 pcf, respectively, from day four to day 56 after LCC casting. Both wet and dry weight increased with time at a decreasing rate, indicating

that cement hydration continued even up to 56 days after LCC casting. In addition, the difference between wet and dry weights increased over time, suggesting that water absorption of LCC increased over time. Figure 2.4 shows that the unconfined compressive strength of LCC also increased over time at a decreasing rate (from 89 psi at day 3 to 179 psi at day 56). According to Tiwari et al. (2017) and Taylor and Halsted (2021), LCC in this study was classified as Class II based on unit weight. As shown in Figure 2.4, the unconfined compressive strength at day 28 was approximately 158 psi, which was within the typical unconfined compressive strength of Class II LCC (i.e., 38.44–240.33 psi).

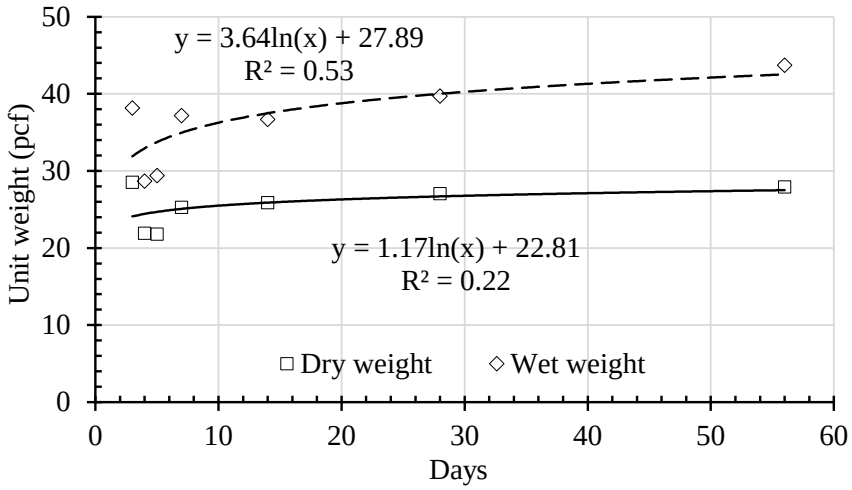

Figure 2.3: Unit Weight of LCC Over Time

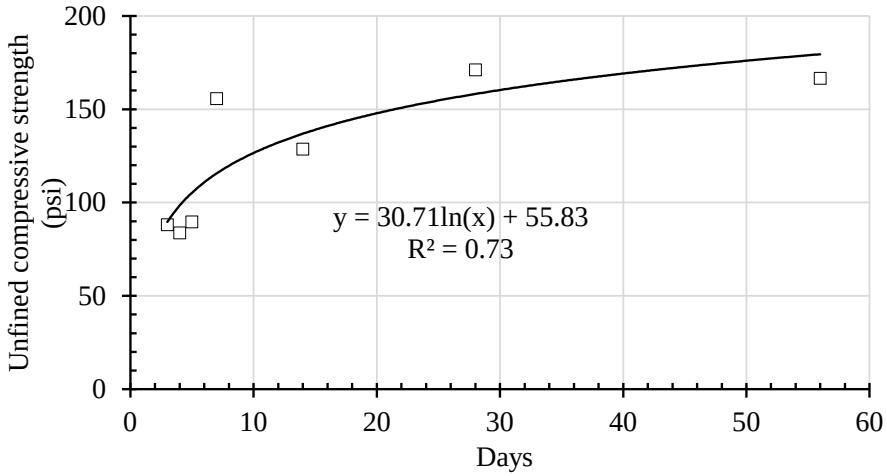

Figure 2.4: Unconfined Compressive Strength of LCC Over Time

2.4 Ribbed Steel Strip Reinforcement

This project used ribbed steel strips from The Reinforced Earth Company. The strips were 2 in. wide by 0.16 in. thick, with a pattern of ribs to increase interaction with backfill material. Galvanization was used for corrosion protection to achieve a design life of at least 75 years. According to Jayawickrama et al. (2015), the yield and tensile strengths of this strip were 80 and 103 ksi, respectively. Figure 2.5 shows placement of the second LCC layer on September 29, 2020. Each steel strip was placed on top of at least two chairs, and the chair bases were inserted into the ground or the prior LCC layer. Chair heights were adjusted to ensure the steel strips were horizontal during strip installation.

Figure 2.5: Placement of the Second LCC Layer

Figure 2.6 shows the front view of seven steel strips installed for the filed pullout tests, and Table 2.2 lists specifics of the steel strips, including when the field pullout tests were conducted. LCC was cast in four layers behind the concrete wall panel facing from September 28 to October 1, 2020. After construction of the concrete pavement above the LCC fill, the front of the

MSE wall (i.e., toe slope) was backfilled with soil to the height of the ground line, as shown in Figures 2.1 and 2.2. Due to the series of elevations of the seven test steel strips that resulted in their installation within different LCC layers, they were installed on two different days. Steel strips #3 and #4 were installed on September 29, 2020, while the other five strips were installed on September 30, 2020. Six of the test strips were 4.5 ft long and one strip (#5) was 11.5 ft long. Ten tests were conducted on seven steel strips, and long-term (one-half and one year) pullout resistances were measured using strips #6 and #7. Steel strips #1, #2, and #3 were tested twice on different days to investigate the residual strength of interaction between steel strips and LCC after an initial loading to failure.

For each steel strip, a hole with a diameter of 5 in. was drilled into the concrete panel (wall facing) to provide access during pullout testing. The front end of the steel strip was inserted into the facing hole. To avoid LCC leaking through the facing hole, gaps between the steel strip and the hole were filled with spray foam, which was removed before the field pullout tests.

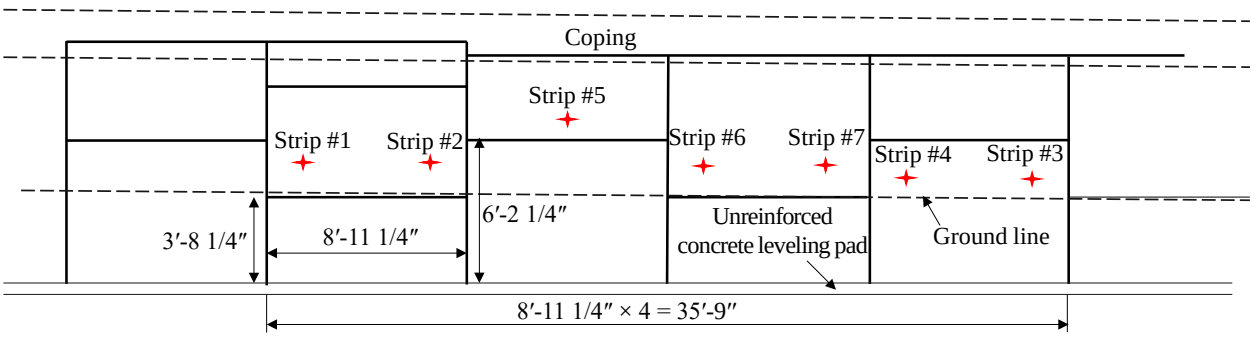

Figure 2.6: Layout of Steel Strips for Field Pullout Tests (Front View)

Table 2.2: Information for Steel Strips and Pullout Tests

Strip No.	Installation date	Test date	Retest date	Length of strip (ft)	Elevation (ft)
#1	09/30/2020	10/03/2020	10/30/2020	4.5	6.3
#2	09/30/2020	10/07/2020	10/30/2020	4.5	6.4
#3	09/29/2020	10/13/2020	10/30/2020	4.5	5.0
#4	09/29/2021	10/30/2020		4.5	4.9
#5	09/30/2020	10/30/2020		11.5	7.6
#6	09/30/2020	04/15/2021		4.5	5.9
#7	09/30/2020	11/05/2021		4.5	6.0

Note. Elevation was from the top of the concrete leveling pad.

2.5 Instrumentation

Figure 2.7 shows the layout of earth pressure cells, temperature sensors (or thermistors), strain gauges, and shape arrays in the instrumented section, which was in the middle of the third column (from left to right) as shown in Figure 2.1. The 10 vibrating-wire earth pressure cells (Model LPTPC09-V from RST Instruments Ltd.) could measure earth pressures up to 51 psi and temperatures ranging from -4 to 176 °F. Five cells were placed on the ground surface horizontally prior to LCC placement to measure vertical earth pressures at distances of 1.4 (EPC-05), 3.3 (EPC-04), 5.3 (EPC-03), 9.2 (EPC-02), and 12.5 ft (EPC-01) from the back facing of the wall panels. The other five cells were installed on the back facing of the wall panels at heights of 1.25 (EPC-06), 2.50 (EPC-07), 5.00 (EPC-08), 7.50 (EPC-09), and 8.75 ft (EPC-10) from the top of the leveling pad to measure lateral earth pressures on the back facing of the wall panels. For EPC-01 to EPC-05, a layer of sand was placed into a shallow circular depression excavated for that purpose. Each earth pressure cell was placed on top of the compacted sand layer, while cells to measure lateral earth pressures were glued to the back facing of the wall panels with supplemental support from Z-shaped connectors anchored in the wall panels with screws. A total of four temperature sensors (model TH0003-250-2) were installed in the LCC to measure LCC temperature changes.

Two temperature sensors (TS-1 and TS-2) were installed in the first LCC layer at a height of 2.3 ft, while the other two temperature sensors (TS-3 and TS-4) were installed in the third LCC layer at a height of 8.0 ft. Temperature sensors TS-1 and TS-3 were 5.0 ft from the back facing of the wall panels, while temperature sensors TS-2 and TS-4 were 10.0 ft from the back facing of the wall panels. The temperature sensors were installed in the LCC layer that had been placed the previous day before placement of the next LCC layer. To install a sensor, a hole with a diameter of 0.4 in. and a depth of 6 in. was drilled into the LCC layer placed on the preceding day; the sensor was installed in the hole, the hole was sealed, and the new LCC lift for the current day was placed. The temperature sensor wire was zip-tied to steel rebar driven into the existing LCC to minimize temperature sensor movement during placement of the next LCC layer.

Two shape arrays with 10 in. long sensing segments were used to measure ground settlements and wall facing deformations. SA-1 was installed horizontally at a height of 6.7 in. from the top of the leveling pad to measure ground settlements, while SA-2 was installed vertically

and adjacent to the back facing of the wall panels to measure wall-facing deformations. In addition, strain gauges (Model C4A-06-125SL-350-39P from Vishay Precision Group, Inc.) were attached to five positions on each of five steel strips to measure changes of axial forces along the length of the steel strip. Since the steel strip could resist some bending moments, strain gauges were attached to both sides of the steel strip. However, due to limited channels on the datalogger, no strain gauges were attached to the bottom side of the rear ends of the lowest two strips (i.e., strips #4 and #5).

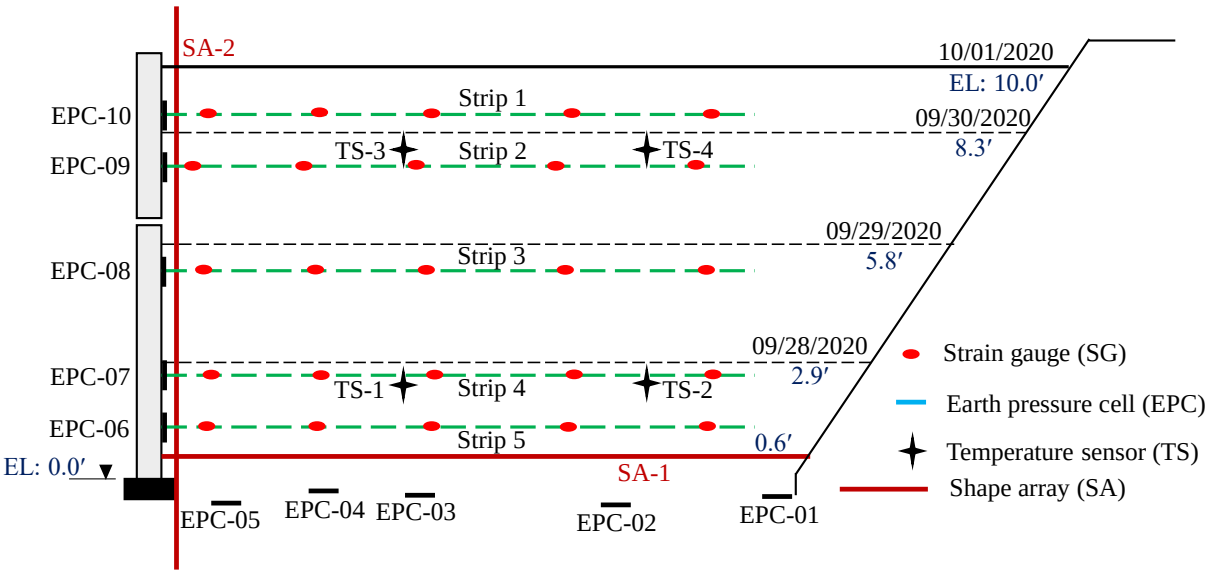

Figure 2.7: Layout of Instrumentation

Dataloggers from Campbell Scientific, Inc., were used to collect and store the data. The earth pressure cells and temperature sensors were connected to an AM16/32 multiplexer, and the collected data were stored in a CR6 datalogger, while the 48 strain gauges were connected to three AM16/32 multiplexers that each had a 4WFBS120 to form a full bridge for the quarter-bridge strain gauge. The data were stored in a CR1000 datalogger. The CR6 and CR1000 dataloggers were each powered by a 12-V battery charged by a solar panel, and the two data loggers took readings of each sensor every 20 minutes.

Figure 2.8 shows the top view of 10 survey targets glued to the wall panels before backfilling. Six survey targets were glued to the left and the right AG-MSE walls adjacent to the LCC-MSE wall, while four survey targets were glued to the LCC-MSE wall. A total station was

utilized to periodically measure positions of these survey targets so settlements and deformations of wall facings over time could be calculated.

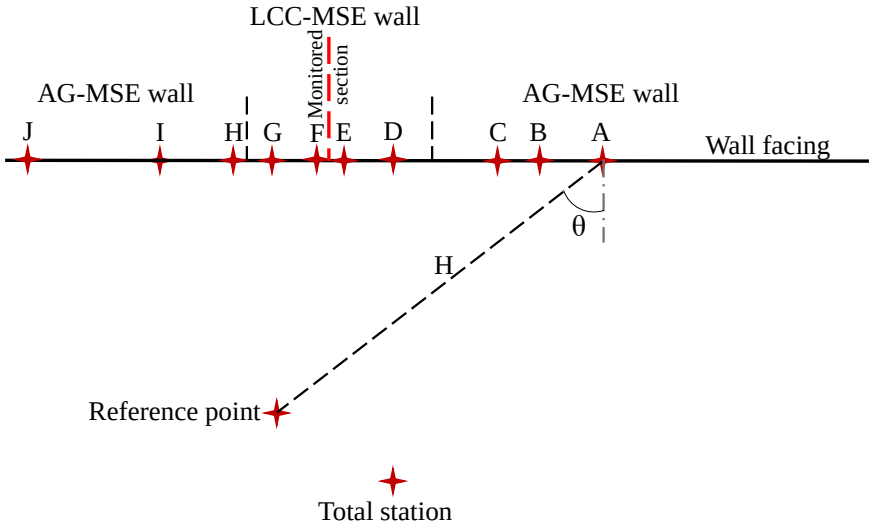

Figure 2.8: Top View of Reference Point, Total Station, and Survey Targets

2.6 Data Reduction

Because cement hydration in LCC emits heat, thereby increasing the LCC temperature, this project had to account for the effects of temperature on the readings of the earth pressure cells. Total pressures measured by the cells after temperature corrections were calculated using Equation 2.1 (GEOKON, 2021).

$$P_{correct} = (R_1 - R_0)G + (T_1 - T_0)K$$

Equation 2.1

Where R_1 and R_0 are current and initial zero readings of digits, respectively; T_1 and T_0 are current and initial zero readings of temperature, respectively; *G* is a linear calibration factor; and *K* is the thermal factor.

As mentioned, the 4WFBS120 completed a full Wheatstone bridge for the quarter-bridge strain gauge. The actual readout of the full-bridge instruction was in millivolts output per volt of excitation. Strain (ε) could then be calculated from these readings using Equation 2.2 (Campbell Scientific, 2017).

$$\varepsilon = \frac{4V_r}{GF(1 - 2V_r)}$$

Equation 2.2

Where V_r is the ratio of output voltage to the excitation voltage, and *GF* is the gauge factor of strain gauge (i.e., 2.09 for strain gauges in this study).

Strain was measured on both sides of the steel strip for a given position, and then the axial force (*F*) and bending moment (*M*) at this position could be calculated from the strain at the bottom side (ε_B) and the strain at the top side (ε_T) using Equations 2.3 and 2.4, respectively.

$$F = \frac{EA(\varepsilon_T + \varepsilon_B)}{2}$$

Equation 2.3

$$M = \frac{EA(\varepsilon_T - \varepsilon_B)I_y}{h}$$

Equation 2.4

Where *E* is the elastic modulus of the steel strip (29,000 ksi), *A* is the area of the cross section of the steel strip (0.31 in^2), *h* is the thickness of the steel strip (0.16 inches), and I_y is the moment of inertia of the steel strip to the weak axis of its cross section (i.e., 0.64 inches^4).

For each survey target, the total station read slope distance (*S*), vertical angle (*ZA*), and horizontal angle (*HA*), as shown in Figure 2.9. Assuming the origin was at the position of the total station, the horizontal plane was the x-y plane, and the x-axis was the line from the total station to the x-y coordinate directly below the reference point. The positions of reference point and the survey target were calculated using Equations 2.5–2.10.

$$x_r = H_r = S_r \cos(ZA_r)$$

Equation 2.5

$$y_r = 0$$

Equation 2.6

$$z_r = V_r = S_r \sin(ZA_r)$$

Equation 2.7

$$x_t = H_t cos(HAR) = S_t \cos(ZA_t) \cos(HAR)$$

Equation 2.8

$$y_t = -H_t sin(HAR) = -S_t \cos(ZA_t)\, sin(HAR)$$

Equation 2.9

$$z_t = V_t = S_t \sin(ZA_t)$$

Equation 2.10

Where (x_r, y_r, z_r) and (x_t, y_t, z_t) are positions of the reference point and the target, respectively; ZA_r, ZA_t are vertical angles of the reference point and the target, respectively; S_r and S_t are slope distances of the reference point and the target, respectively; and HAR is the horizontal angle difference between the reference point and the target.

Then the position of the target relative to the reference point could be calculated using Equations 2.11–2.13.

$$\Delta x = S_t \cos(ZA_t) \cos(HAR) - S_r \cos(ZA_r)$$

Equation 2.11

$$\Delta y = -S_t \cos(ZA_t)\, sin(HAR)$$

Equation 2.12

$$\Delta z = S_t \sin(ZA_t) - S_r \sin(ZA_r)$$

Equation 2.13

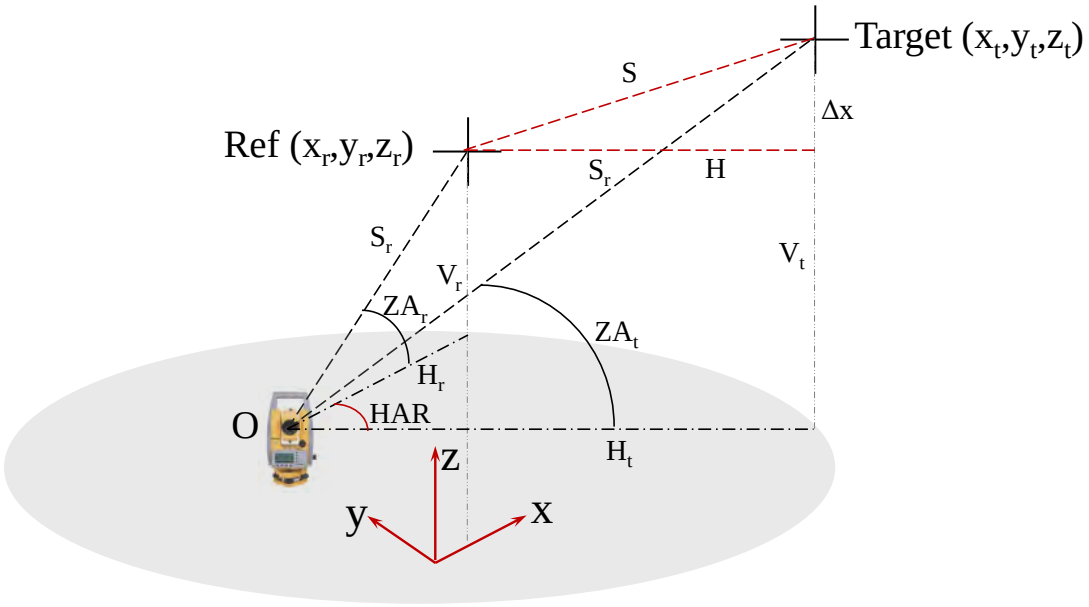

Figure 2.9: Method for Reading Survey Targets

The distance between the reference point and the target was calculated using Equation 2.14. As shown in Figure 2.9, if the horizontal angle between the normal direction of the wall facing and

the direction from the target to the reference point was θ, then the distance between the reference point and the target in the normal direction of the wall facing could be calculated using Equation 2.15. Therefore, changes of values calculated by Equations 2.13 and 2.15 were wall settlements and wall facing deformations.

$$H = \sqrt{\Delta x^2 + \Delta y^2} = \sqrt{(S_t \cos(ZA_t)\cos(HAR) - S_r \cos(ZA_r))^2 + (-S_t \cos(ZA_t)\, sin(HAR))^2}$$

Equation 2.14

$$H_n = Hcos\theta$$

Equation 2.15

Chapter 3: Field Pullout Tests

This chapter contains a description of the methodology for conducting field pullout tests of steel strips encased in LCC. The effects of curing, strip length, and remobilization after initial failure on the pullout capacities were investigated. The results of 10 pullout tests conducted on seven steel strips are presented and analyzed. Of the seven steel strips, six strips were 4.5 ft in length, and one was 11.5 ft long. The six short strips were pulled out after different curing periods, and three short strips were repulled after their initial pullout tests.

3.1 Test Setup

Figure 3.1(a) shows the test device designed for the field pullout test. A hollow cylinder was used to pull out the steel strip against the wall facing. An extension consisting of a steel pipe with an inner diameter of 6 inches, length of 18 inches, and steel flanges on both ends was bolted to the hollow cylinder to create space for the load cell and the front end of the steel strip to move horizontally. Since the front surface of the concrete panel was rough, mortar was used to smooth the wall-facing surface to supply a platform for the extension flange. One end of the load cell was connected to the front end of the steel strip via a fitting with a pin connection, while the other end was connected via the 3-ft-long threaded rod. A steel plate (plate C) was connected to the hard cap of the hollow cylinder using two bolts, and a center hole in plate C enabled the threaded rod to pass through the plate. Finally, a nut larger than the hole in plate C was used to tighten the threaded rod against plate C. The threaded rod, load cell, and steel strip could move together with the hard cap when the cylinder was extended by a hand pump.

Figure 3.1(b) shows the test setup for a field pullout test. Three ratchet straps were used to support and adjust the position of the hollow cylinder and steel pipe during installation and support the test device during the field pullout test. A displacement transducer independently supported on the ground measured the displacement of the hard cap (i.e., displacement of the front end of the steel test strip), and the load cell was used to measure the force to pull the strip. The strips were pulled out at a rate ranging from 3.94×10^{-4} to 1.57×10^{-3} in./s before reaching peak pulling force and at a rate ranging from 3.94×10^{-3} to 5.9×10^{-3} in./s after reaching peak pulling force.

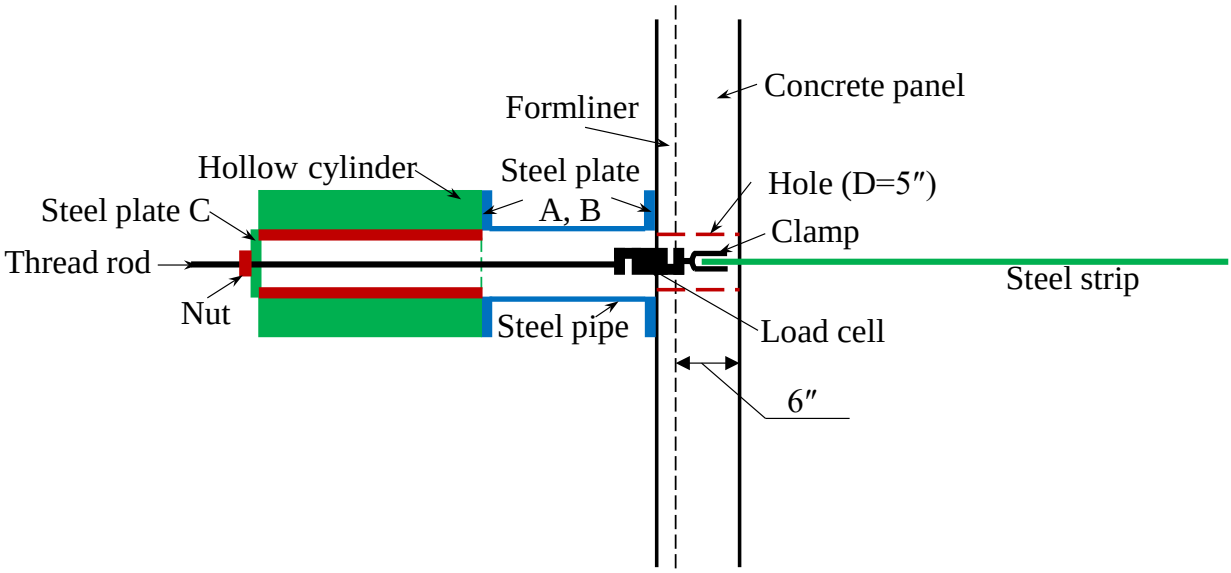

(a) Field Pullout Test Device (not to scale)

(b) Pullout Test Setup in Field

Figure 3.1: (a) Test Device; (b) Setup

3.2 Test Results and Analysis

3.2.1 Temperature Sensor Layout and Measurements for the LCC

Figure 3.2(a) shows the layout of one pressure cell and two thermistors used to monitor LCC temperatures. A pressure cell (Point A) was attached to the back of the wall facing on September 26, 2020, while the first lift of LCC was cast on September 28, 2020. On September 29, 2020, two thermistors (Points B and C) were inserted into the first lift (5 ft and 10 ft from the back of the wall facing, respectively) before pouring the second lift of LCC on that day. Since the rear ends of strips #1–4 were 4.5 ft from the back of the wall facing, the temperature recorded by the pressure cell and the thermistor (Point B), located 4.5 ft from the back of the wall facing, represented temperature changes at the front and rear ends of the strip, respectively. The embedded length of strip #5 was 11.5 ft, so the temperatures from Points A, B, and C represented temperature changes at the front end, middle, and rear end of this long strip.

Figure 3.2(b) shows temperature change behind the wall facing and in the LCC over time. After pouring the second lift of LCC, temperatures behind the back of the wall facing and in the LCC reached their peaks in one day. Thermal conductivity of the wall facing caused the temperature behind the wall to drop much more quickly than the temperatures in the LCC. The temperature behind the wall facing varied with daily temperature variations.

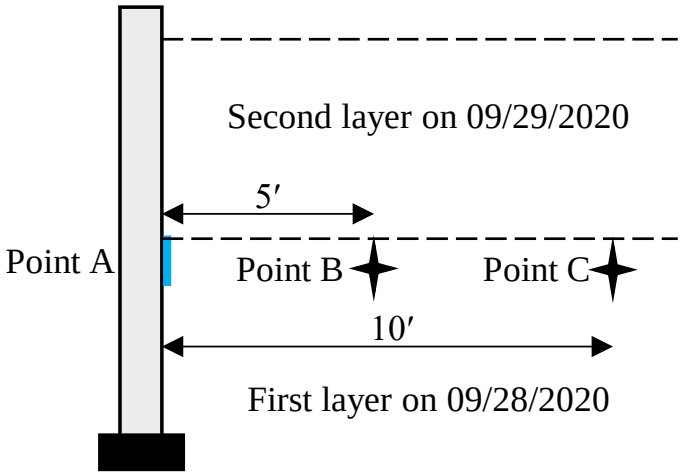

(a) Temperature Sensor Layout

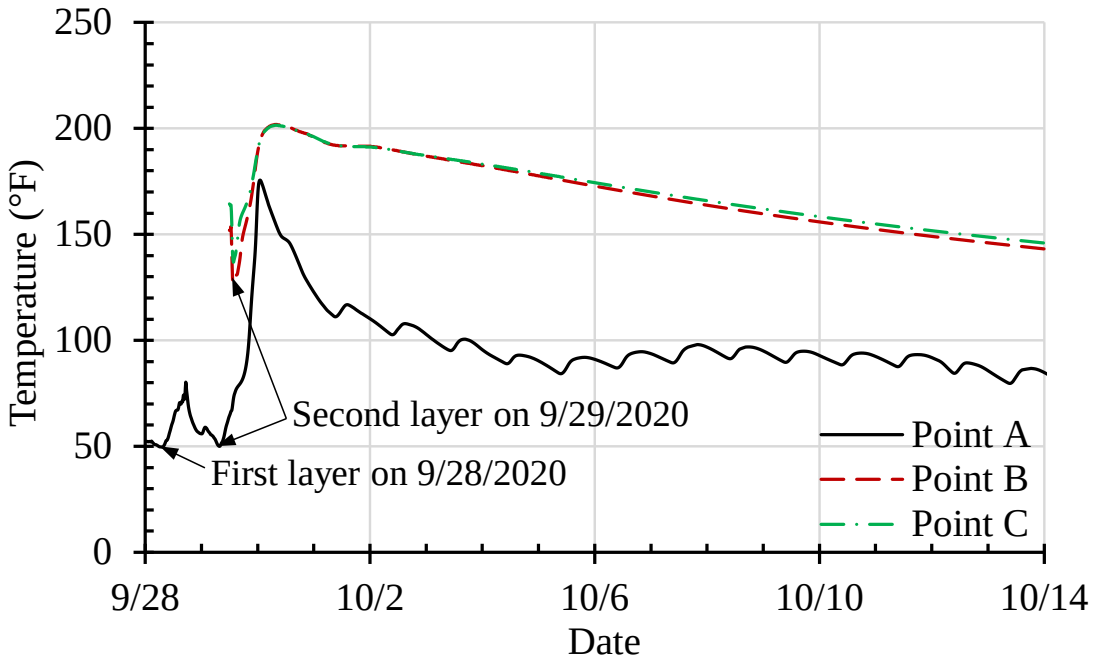

(b) Temperature Change Over Time in LCC

Figure 3.2: (a) Temperature Sensor Layout; (b) Temperature Change over Time in LCC

3.2.2 Pullout Capacity

Pullout capacity exceeded 2,700 lb for all test strips, and capacities were consistent among test strips with curing periods of one month or less. Pullout capacities were substantially higher for test strips with curing periods of 6 months and one year. Figure 3.3 shows the force versus displacement results for the six short strips.

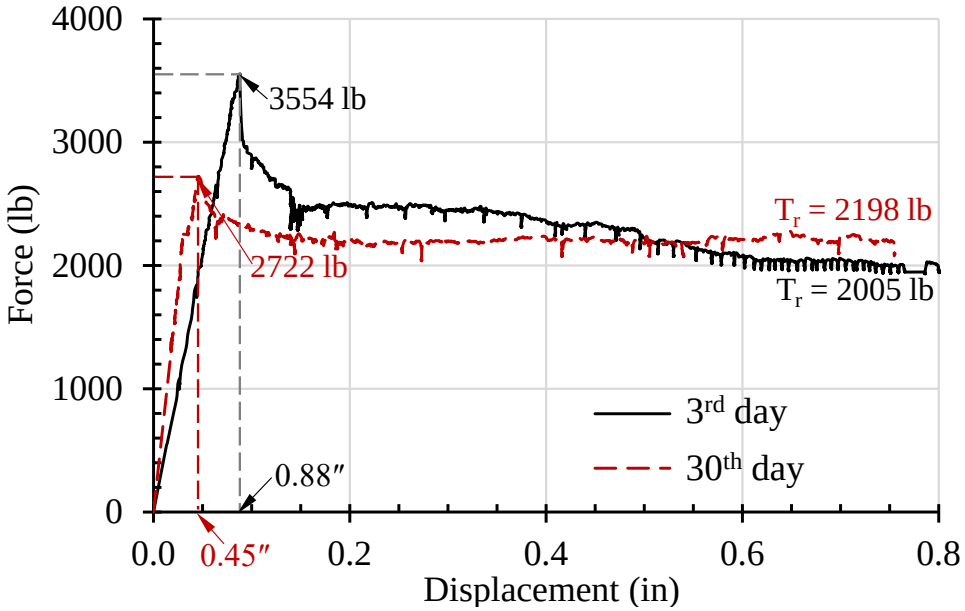

(a) Strip #1 Pulled on Day 3 and Repulled on Day 30

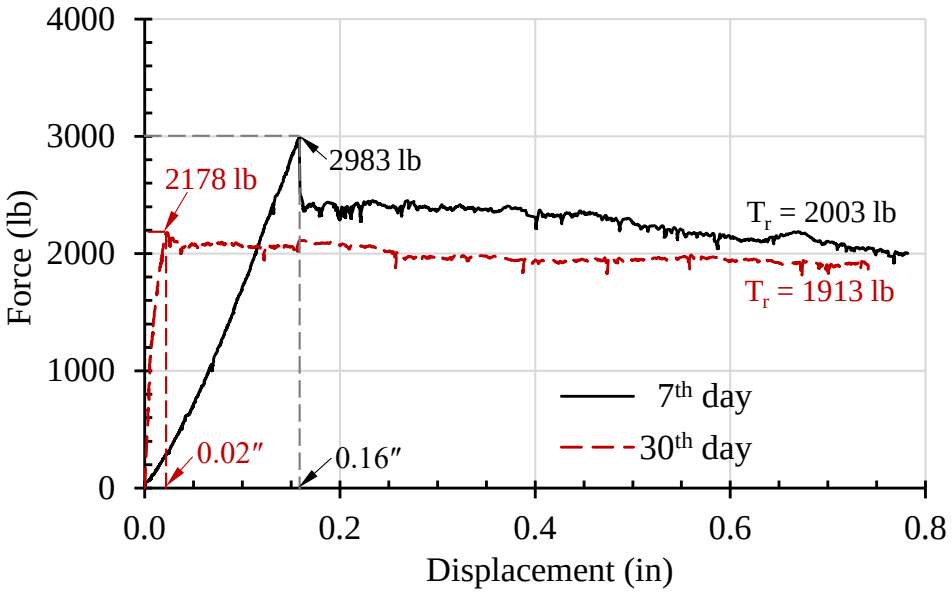

(b) Strip #2 Pulled on Day 7 and Repulled on Day 30

Figure 3.3: Pullout Tests of Short Strips

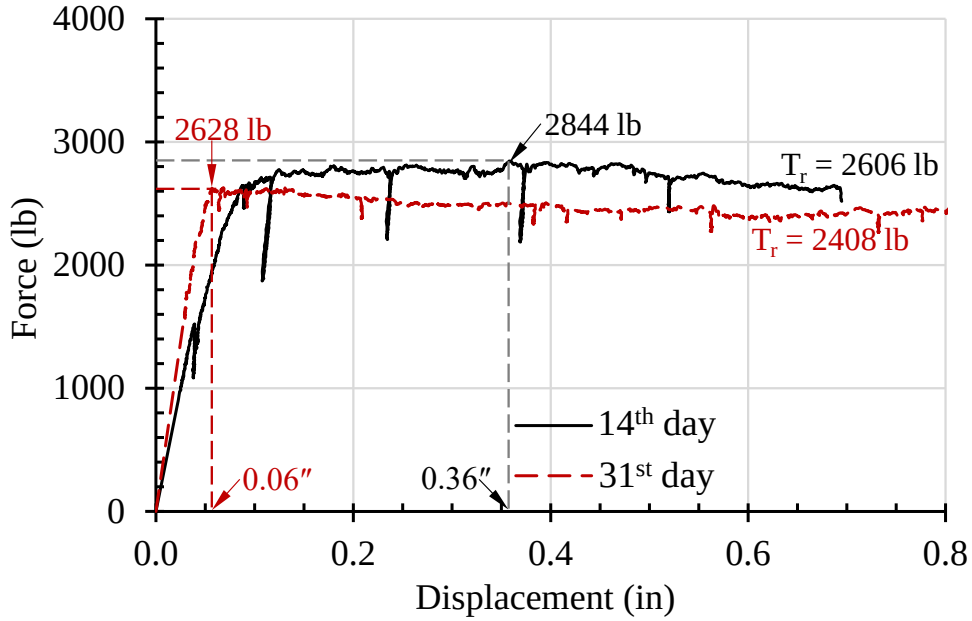

(c) Strip #3 Pulled on Day 14 and Repulled on Day 31

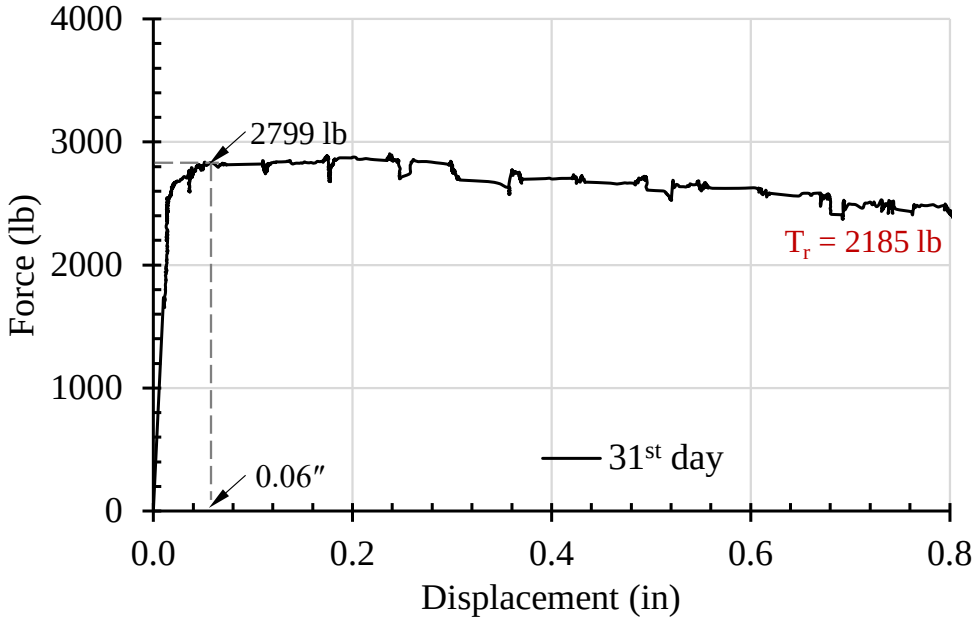

(d) Strip #4 Pulled on Day 31

Figure 3.3: Pullout Tests of Short Strips (Continued)

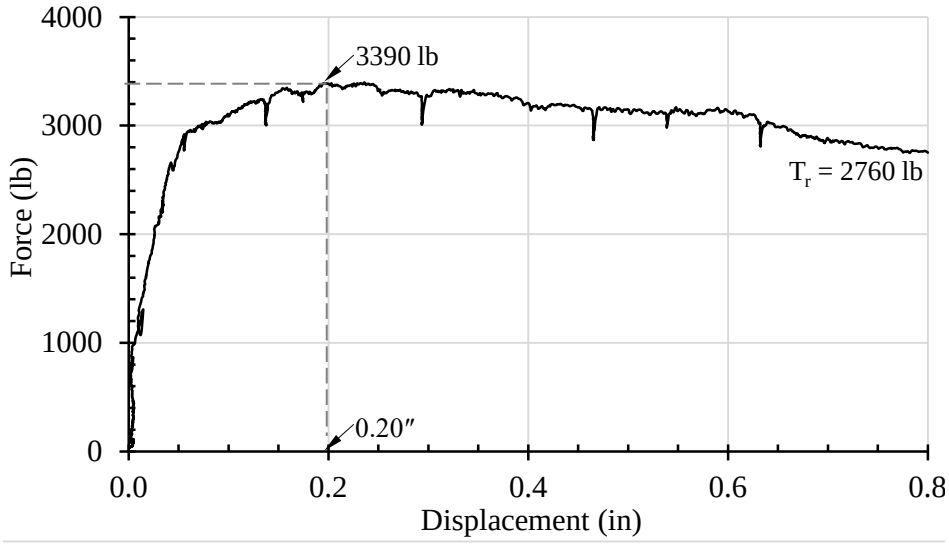

(e) Strip #6 Pulled on Day 197

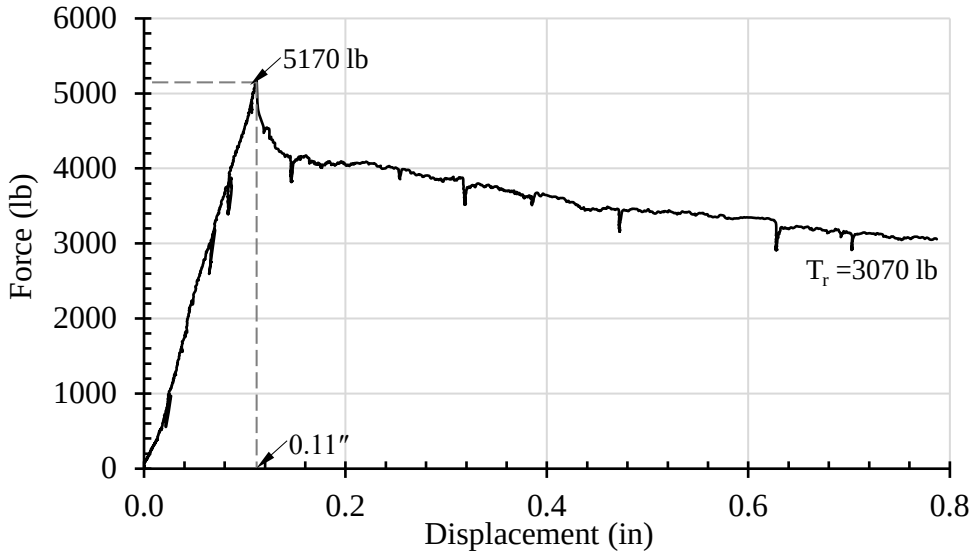

(f) Strip #7 Pulled on Day 401

Figure 3.3: Pullout Tests of Short Strips (Continued)

As shown in Figure 3.3, the load-displacement curves had two distinct shapes. All tests had relatively high strengths up to very large displacements (0.8 in.), but some tests had a very high peak stress, a rapid loss of strength, and then steady to slightly declining strength up to very large displacements; other tests did not have a sharp peak. For pullout tests for strip #1 and strip #2 (tested on days 3 and 7 after LCC casting, respectively), the force required to pull the strip initially increased with displacement and then dropped quickly (approximately 30% and 19%, respectively)

after reaching peak force, followed by gradually decreasing force to a stable value as displacement increased. However, for strips #3 and #4, which were tested on days 14 and 30 after LCC casting, respectively, the force dropped gradually to a constant value after reaching peak force as displacement increased. No abrupt drops of pulling force were observed for the two strips as with the longer strip (strip #5) (Figure 3.4).

Strips #6 and #7 were tested on day 197 and day 401, respectively, to investigate the long-term pullout resistance of steel strips in LCC. No abrupt drop of pulling force after reaching peak force was observed on day 197, but an abrupt drop was observed on day 401. After reaching peak force, the pullout resistance of many strips consisted of two stages due to shear-off failure (i.e., quick drop of pulling force after reaching peak value) and pullout failure (i.e., gradual decrease of pulling force with displacement of steel strip) as described by Sayadi et al. (2016a).

Figure 3.4 shows various post-peak behaviors after different curing periods. The cause of prominent peak/quick drop-off in strength after curing periods of three and seven days may be due to additional normal stress on the steel strip induced by high temperature in the LCC. This normal stress decreased after the LCC de-bonded from the strip during shear. However, for curing periods of 14 days or longer, the thermally induced normal stress decreased substantially due to decreased LCC temperatures, meaning no prominent peak in resistance and then a quick drop after peak resistance occurred for tests from day 14 to day 197. Although the peak resistance was observed for the final test on November 5, 2021, the very high peak and quick drop-off may be temperature and/or curing related, but more research is needed to determine if the peak and drop-off was a real event or an artifact of this test.

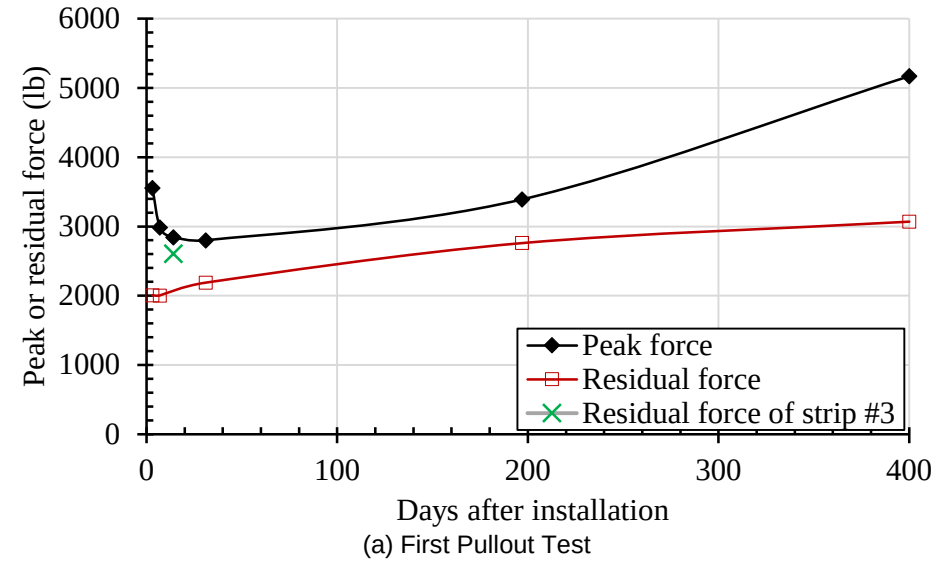

(a) First Pullout Test

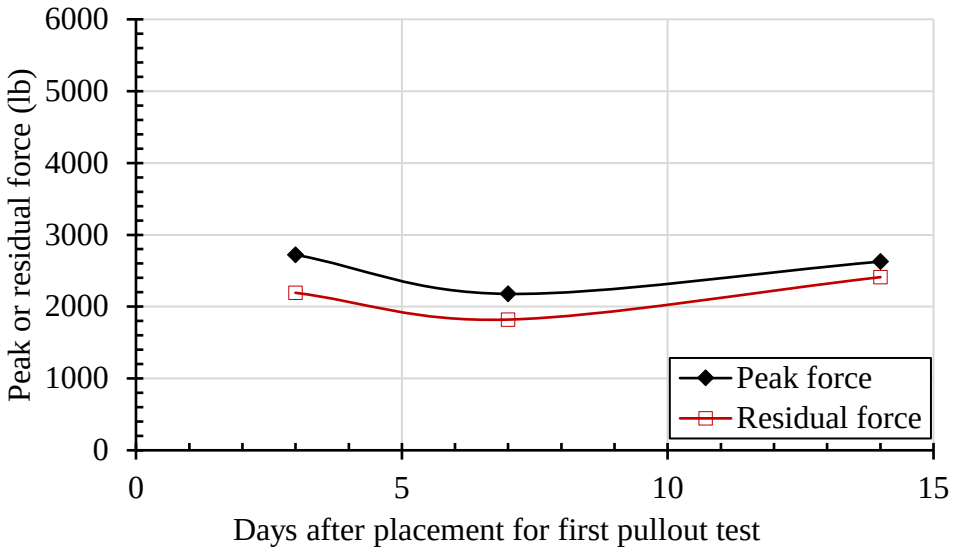

(b) Repull Pullout Test

Figure 3.4: Change of Peak and Residual Forces Over Time

Figure 3.4 also shows peak and residual forces for the initial and repull pullout tests. Figure 3.4(a) shows that the peak force decreased within 14 days after LCC casting and remained constant from day 14 to day 31, after which the peak force increased over time. Due to the decrease in temperature (Figure 3.2), additional normal stress caused by LCC expansion on the steel strip decreased, potentially causing the peak force required to pull the strip to decrease over the first two weeks after LCC casting. The residual force was very consistent from the third day after LCC casting for strips #1, #2, and #4, as shown in Figure 3.4(a), indicating that the residual interaction

between LCC and the strips did not change significantly within the first month after the LCC was cast. Increasing pullout resistance was also measured for strips #5, #6, and #7 as the curing time increased. Although the reason for the increased residual force of strip #3 is unclear, additional resistance from the chairs used to support the strips during installation may have been a factor. The steel strip was tied to the chairs with steel wires, meaning the chair may have hooked a rib and been forced to move together with the strip after some displacement, thereby increasing the pullout resistance of strip #3.

Figure 3.4(b) shows that the peak and residual repull forces measured for strip #2 were somewhat lower than the values for strip #1 and strip #3. Strip #1 was tested on day 3 and retested on day 31; the interface between strip #1 and LCC was expected to gain strength over that time, and the strength-increase rate was expected to decrease over time for the residual force. The long period of recovery for strip #1 (28 days) and the additional early days (days 3–7) in the recovery period explain why the peak and residual strengths during the repull pullout tests were higher for strip #1 than strip #2. As mentioned, the chairs may have moved with strip #3, leading to the higher peak and residual repull forces for strip #3 than strip #2.

Figure 3.5 shows the force versus displacement curve for the long strip (strip #5). The displacement transducer slipped out from steel plate C during testing of strip #5, so displacement in Figure 3.5 was evaluated based on the pullout velocity for the other four steel strips tested on the same day (October 30, 2020). For strip #5, the peak force of the first pullout test was 4,982 lb, which was 1.78 times the peak force for strip #4, but the length of strip #5 was 2.55 times the length of strip #4, meaning the peak force did not increase linearly with the length of the steel strip. The low pullout capacity for the long steel strip may be due to the different magnitudes of movement of the steel strip from the front to the end, meaning the peak interface strengths along the steel strip length may not have been mobilized at the same time.

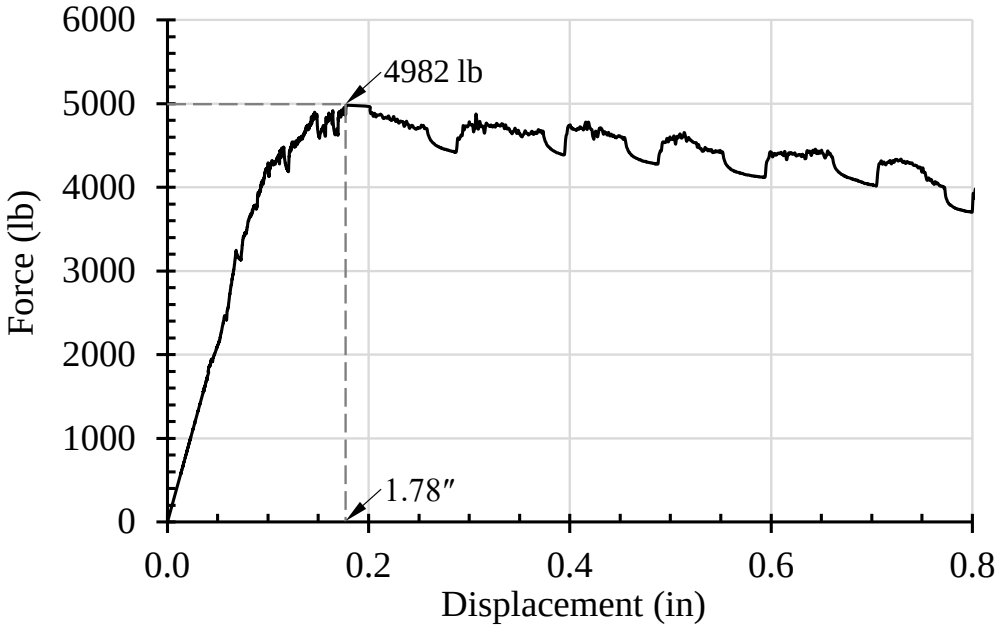

Figure 3.5: Pullout Test of Long Strip (Strip #5)

3.3 Discussion

The interaction of the ribbed steel strip with cohesionless backfill material differed from its interaction with cohesive material since most of the strip's peak strength comes from the strength of cementitious bonding. AASHTO (2012) and Berg et al. (2009) suggested the pullout capacity of a steel strip in cohesionless material could be calculated by Equation 3.1.

$$T_p = 2F^* L_e W_e \sigma_v$$

Equation 3.1

Where T_p is the pullout capacity of steel strip (kN); F^* is the pullout resistance factor; L_e and W_e are the effective length (m) and width (m) of the steel strip, respectively; and σ_v is the effective overburden stress of the steel strip. For the ribbed steel strip, the pullout resistance factor depends on the buried depth of the steel strip, peak friction angle, and coefficient of uniformity (C_u) of backfill material.

When the buried depth of the steel strip is less than 20 ft, the pullout resistance factor is

$$F^* = 1.2 + \log(C_u) \leq 2.0$$

Equation 3.2

However, if the buried depth is more than 20 ft, the factor depends on the friction angle of the aggregate (φ) as

$$F^* = tan\varphi$$

Equation 3.3

Weldu et al. (2016) conducted lab pullout tests for a ribbed steel strip buried in aggregates (approximate relative compaction of 94%) with various coefficients of uniformity under various normal stresses. Jayawickrama, Surles, Wood, and Lawson (2013) also conducted lab pullout tests with various degrees of relative compaction of aggregate backfill, lengths of steel strip, and normal stresses for ribbed steel strips, while Ye et al. (2022) conducted lab tests of steel strips encased in LCC under normal stresses of 209, 627, and 1,253 psf. Figure 3.6 shows pullout resistance factors calculated from pullout test results in LCC (75% cement and 25% fly ash) from lab and field pullout tests and in aggregates from lab pullout tests, as well as recommendations from AASHTO (2012), in which a coefficient of uniformity of four and an aggregate friction angle of 34° were used to calculate the pullout resistance factor. The unit weight of LCC and aggregate were assumed to be 32 and 127 pcf, respectively. Pullout resistance factors in LCC were larger than the values in aggregates, as shown in Figure 3.6, particularly for low normal stresses (minimal depths). Based on these results, a substantial portion, possibly the dominant portion, of LCC peak strength is a result of cohesion rather than frictional interaction among particles. Therefore, the difference between the pullout force of strips between aggregate and LCC decreased as depth increased, meaning the pullout capacity of the strip in aggregate exceeded the capacity of LCC.

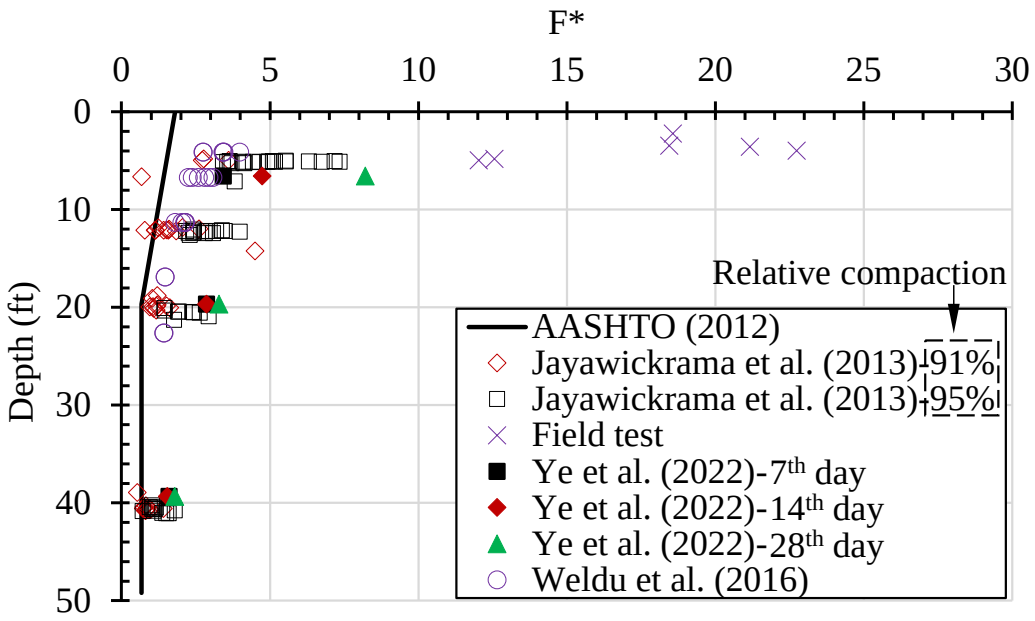

Figure 3.6: Comparison of LCC Field Tests and Aggregate

3.4 Conclusions

Ten field pullout tests of seven strips embedded in an LCC-MSE wall were conducted. Pullout capacity exceeded 2,700 lb for all test strips, and test strip capacities were consistent with curing periods of one month or less. Pullout capacities were substantially higher for test strips with curing periods of six months and one year and were much higher than pullout tests in aggregate with similar overburden pressures.

In the initial pullout test, pullout capacity of a steel strip in LCC decreased slightly within 14 days after LCC casting and remained constant within the first month after LCC casting. The LCC temperature peaked the first day after casting and then decreased gradually. The high temperatures may have caused a temporary, thermally induced increase in normal stress on the steel strip, resulting in an elevated pullout capacity for the three-day test. Overall, initial pullout capacity of a steel strip increased over time due to cement hydration.

In the repull test, the peak and residual forces of strip #1 (initial pullout test at day 3) were somewhat larger than the forces for strip #2 (initial pullout test at day 7). The extended curing period for strip #1 may have increased interface strength between strip #1 and LCC. However, the pullout capacity of the strip in LCC did not increase linearly with strip length, potentially due to differential movement of the strip along the length.

Chapter 4: MSE Wall Construction and LCC Curing

This chapter details the instrumentation of the LCC-MSE wall with earth pressure cells, strain gauges, thermistors, and shape arrays. The monitoring data during construction of the LCC-MSE wall and the first month after construction (LCC curing) were analyzed to investigate the short-term performance of the LCC-MSE wall. The wall performed well during this period with minimal lateral and vertical deformations.

4.1 Pressure and Temperature

Figures 4.1 and 4.2 show pressures and temperatures, respectively, at the base of the LCC backfill and at the back facing of the wall panels during LCC placement.

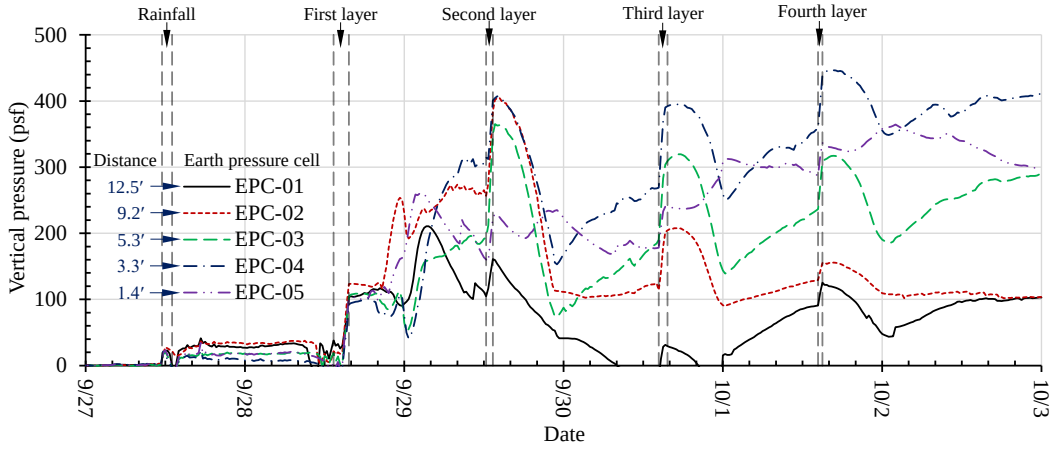

(a) At the Base of LCC Backfill

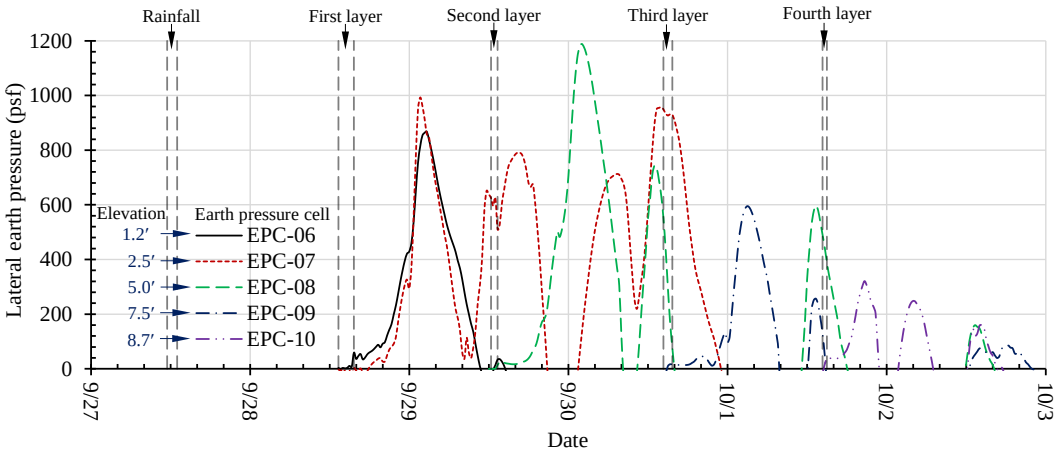

(b) At the Back Facing of Wall Panels

Figure 4.1: Pressures during LCC Placement

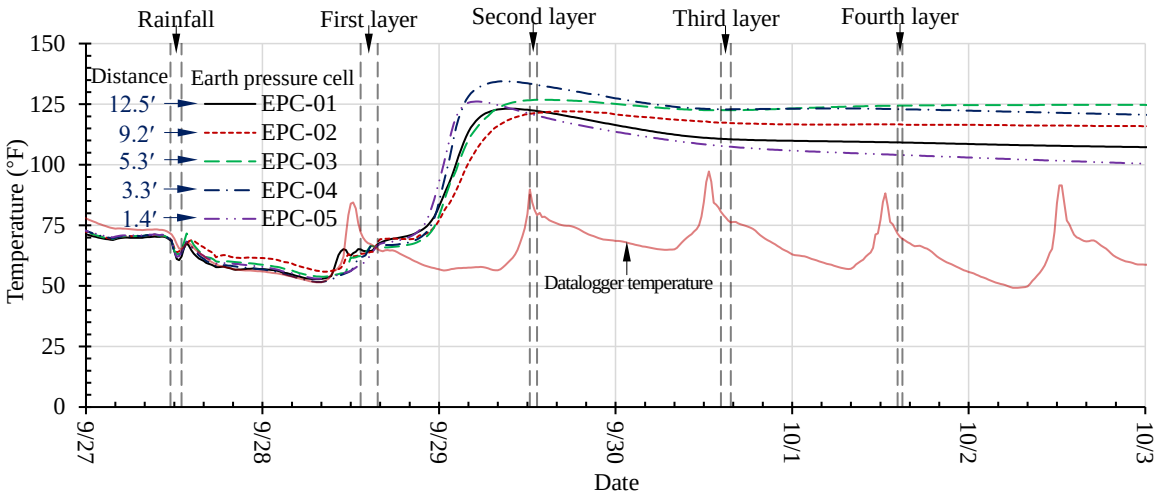

(a) At the Base of LCC Backfill

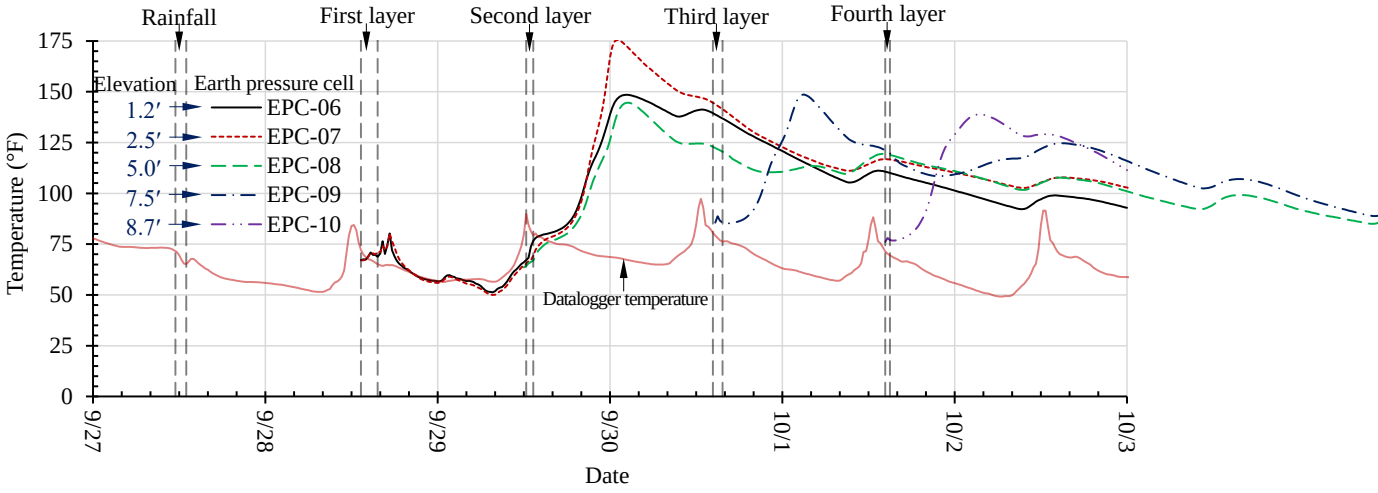

(b) At the Back Facing of Wall Panels

Figure 4.2: Temperatures during LCC Placement

Earth pressure cells EPC-01 to EPC-07 were installed on September 26, 2020, while EPC-08, EPC-09, and EPC-10 were installed on September 29, September 30, and September 30, respectively. Heavy rainfall on September 27 caused retained water above EPC-01, EPC-02, EPC-03, EPC-04, and EPC-05. This water was removed on September 28 before the first LCC layer was placed. The water accumulation and removal on the five cells could explain the measured pressure increases on September 27 and pressure reductions on September 28. From 15:40 to 20:00 on September 28, the average pressure reading for the five cells was 104 psf, which matched the weight of the initial LCC layer (1.0 m thick) (32 pcf × 3.23 ft = 103 psf). Comparatively, EPC-06

was 1.7 ft from the top surface of the first LCC layer, and the overburden stress was 54 psf. The average pressure of 48 psf measured by EPC-06 from 15:40 to 18:00 on September 28 indicated that hydraulic pressure was applied to the back facing of the wall panels immediately after LCC placement. Temperatures measured by EPC-01 to EPC-05 peaked at 8:00 on September 29 (16 hours after placement of the first LCC layer), followed by gradually decreasing temperatures over time.

Temperature increases measured by EPC-01, EPC-02, EPC-03, EPC-04, and EPC-05 were attributed to heat generated by cement hydration. Since the wall concrete panels effectively transferred heat from LCC into the atmosphere, temperatures measured by EPC-06 and EPC-07 decreased from 18:00 on September 28 to 8:00 on September 29. In addition, temperature variations in the first LCC layer after placement and during curing may have contributed to the pressure variations measured by EPC-01 to EPC-07 from 20:00 on September 28 to 12:20 on September 29. Pressures measured by EPC-01 to EPC-05 increased during placement of the second LCC layer; EPC-03 (distance of 5.3 ft) measured the largest pressure increase of all five cells. From 17:20 on September 29 (four hours after placement of the second LCC layer), the temperatures measured by EPC-06 to EPC-08 increased rapidly and peaked at 2:00 on September 30 (12 hours after placement of the second LCC layer). Similarly, the average pressure measured by EPC-08 at the elevation of 5.0 ft was 21 psf immediately after placement of the second LCC layer (13:20–17:20 on September 29), which approximately corresponded with hydraulic pressure. Similar readings (i.e., EPC-09 and EPC-10 read the hydraulic pressures of LCC right after placing the third and fourth LCC layers, respectively) were observed after placement of the third and fourth LCC layers.

In contrast to the gradual reduction of temperatures measured by EPC-01 to EPC-05 over time, temperatures measured by EPC-06, EPC-07, EPC-08, EPC-09, and EPC-10 were affected by daily air temperatures. For example, the measured temperatures showed peak values at 12:00 on September 30, October 1, and October 2, 2020, which corresponded to the highest temperatures of these days as measured by the data logger. Since LCC is a good insulator, heat induced by curing of the second, third, and fourth LCC layers did not significantly influence the temperatures measured by EPC-01 to EPC-05, which were buried under the first LCC layer. However, the

temperature measured by EPC-09 (elevation of 7.5 ft) peaked at 4:00 on October 1, while the temperature measured by EPC-08 reached a high value at 5:00 on October 1 and then a peak value at 12:40 on October 2. (The peak value was likely aided by a high ambient air temperature.) In addition, the temperature measured by EPC-10 (elevation of 8.7 ft) reached its peak value at 4:00 on October 2, while the temperature measured by EPC-09 reached a high value at 7:40 on October 2 before reaching its peak value (aided by air temperature) at 12:40 on October 2. Therefore, although heat induced by cement hydration of a newly placed LCC layer could affect the temperature in previous layers, the effect was shown to decline quickly with distance due to the insulative properties of LCC. For example, temperatures measured by EPC-06 and EPC-07 did not reach peak values corresponding to peak values measured by EPC-09 at 4:00 on October 1. Similarly, temperatures measured by EPC-06 to EPC-08 did not reach peak values corresponding to the peak temperature value measured by EPC-10 at 4:00 on October 2.

As shown in Figures 4.1 and 4.2, the pressures and temperatures measured by the pressure cells did not vary significantly within the first four hours after LCC placement, indicating that the setting time of LCC in this project was within the practical setting time range of 2–4 hours as reported by Taylor and Halsted (2021). In addition, the measured temperatures increased to peak values 12–16 hours after LCC placement, indicating that maximum cement hydration also occurred 12–16 hours after LCC placement.

Figures 4.3 and 4.4 show pressures and temperatures, respectively, at the base of the LCC backfill and at the back facing of the wall panels during LCC curing.

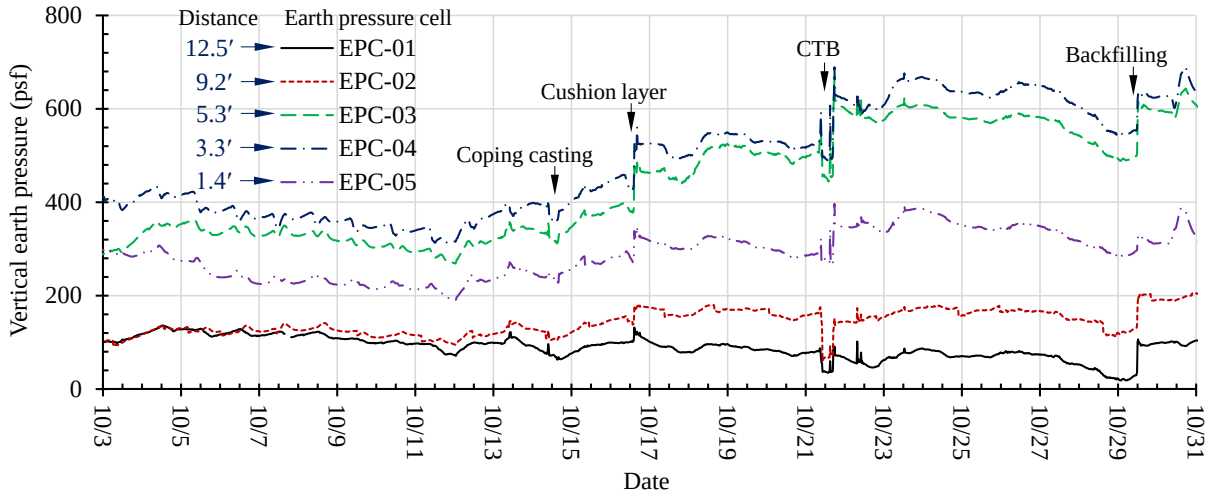

(a) At the Base of LCC Backfill

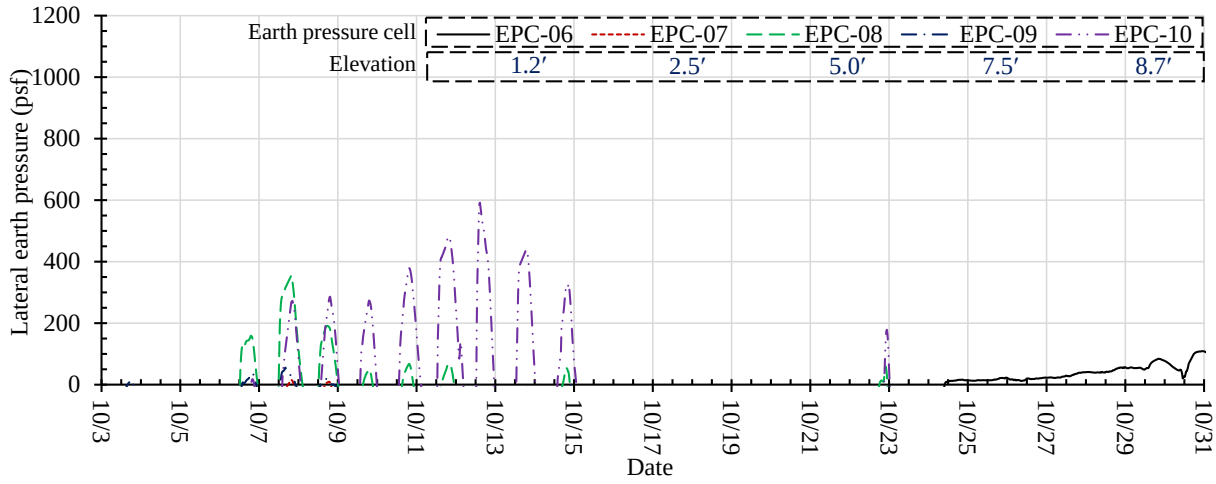

(b) At the Back Facing of Wall Panels

Figure 4.3: Pressures During LCC Curing

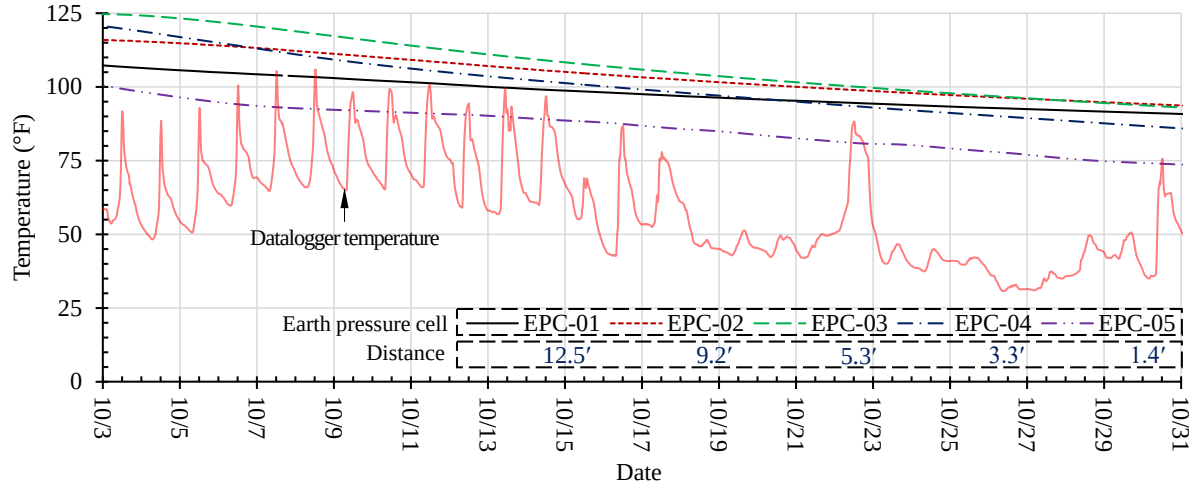

(a) At the Base of LCC Backfill

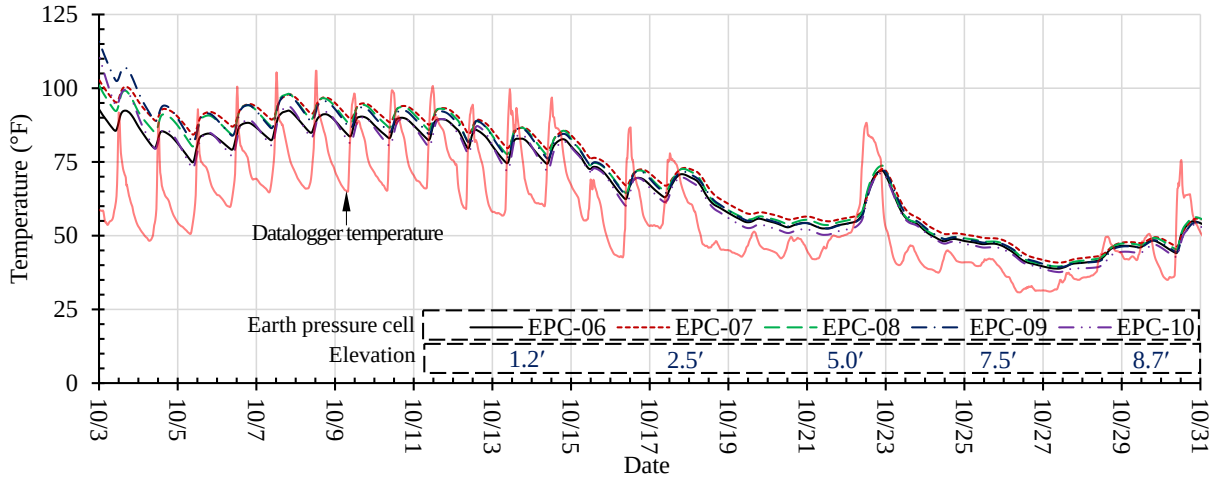

(b) At the Back Facing of the Wall Panels

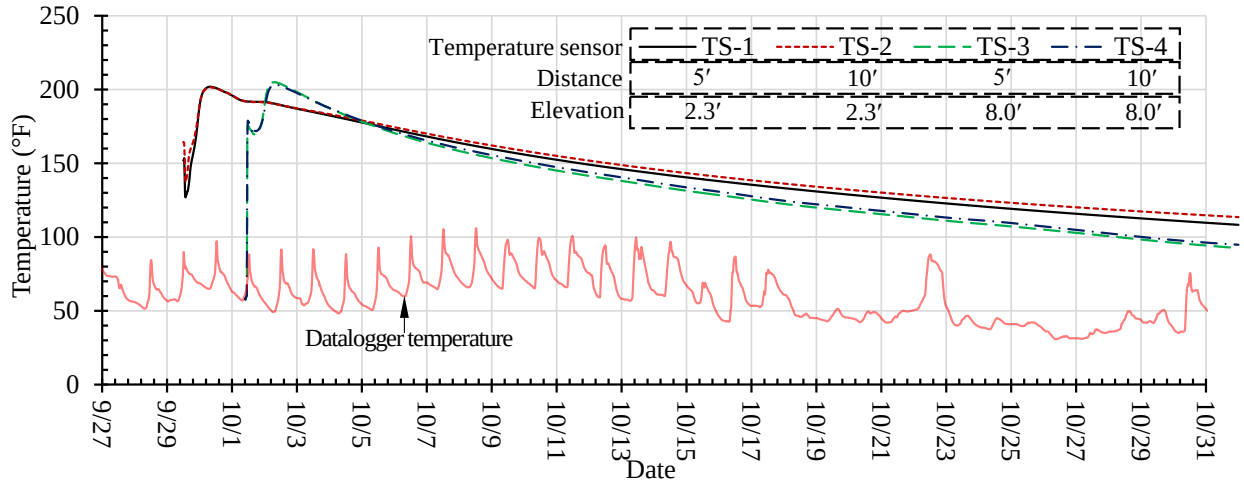

(c) In the Middle of LCC Backfill

Figure 4.4: Temperatures During LCC Curing

As shown in the figures, temperatures at the base of the LCC backfill decreased gradually from October 3 to 31, 2020, due to the decreasing rate of cement hydration. In addition, since EPC-05 (distance of 1.4 ft) and EPC-04 (distance of 3.3 ft) were closer to the wall facing than the other three pressure cells (EPC-01, EPC-02, EPC-03), their measured temperatures decreased over time more quickly than temperatures for EPC-01, EPC-02, and EPC-03. The temperatures measured by EPC-05 were lowest among the five pressure cells. Abrupt pressure changes measured by EPC-01 to EPC-05 matched the stages of construction, such as placement of cushion layer and CTB layer, as shown in Figure 4.3. The vertical pressures increased as the distance from the wall facing increased from 0.41 m to 1.01 m and then decreased until the back of the backfill. The LCC backfill behind the wall facing may have been supported by the footing at the wall face and the slope at that back of the fill, resulting in a higher vertical stress below the center of the backfill (i.e., at EPC-02, EPC-03, and EPC-04).

The measured temperatures at the back facing of the wall panels in the LCC peaked nearest the center of the fill mass. The peak temperatures and pressures at the face lagged the peak values of the internal LCC temperatures recorded by the datalogger because heat transfer requires time. From October 6 to 15, 2020, LCC expansion due to temperature increases likely caused the increase in lateral earth pressures behind the wall panels at elevations of 5 ft and 8.7 ft, as shown in Figure 4.3(b). However, LCC contraction due to decreased air temperature starting on October 15 meant that the lateral earth pressures at the back facing of the wall panels between October 15 and 22 were negligible.

As shown in Figure 4.4(c), the temperature readings from the sensors installed in the LCC layer cast on the previous day initially decreased and then increased due to the newly placed LCC layer. In addition, temperature sensors TS-1 and TS-3, located 5 ft from the back facing of the wall panels, had lower readings than sensors TS-2 and TS-4 at a distance of 10 ft from the panels, indicating that heat conduction through the wall panels helped cool the LCC. In addition, temperature sensors TS-3 and TS-4 in the third LCC layer demonstrated faster temperature reduction rates over time than sensors TS-1 and TS-2 in the first layer, indicating that cooling rates decreased as the distance from the boundary of the mass increased.

4.2 Force and Moment of Strips

Jayawickrama et al. (2015) reported that the yield and tensile strengths of the steel strips adopted in this project were 80 and 103 ksi, respectively. Considering the elastic modulus (E) of the steel strip was 29,000 ksi, the strains corresponding to its yield and tensile strengths were 0.28% and 0.36%, respectively. Equation 4.1 was used to calculate the volt output per excitation volt corresponding to the yield and tensile strength of this strip, which were 1.44×10^{-3} and 1.86×10^{-3}, respectively (Campbell Scientific, 2017).

$$\Delta V_r = \frac{GF \cdot \frac{\sigma}{E}}{4 + 2GF \cdot \frac{\sigma}{E}}$$

Equation 4.1

Since the CR1000 datalogger displayed its measurement in millivolts per volt of excitation, the readings were taken as an indication that something was wrong with the strain gauge, likely due to high temperature in the LCC, if the readout change of the strain gauge after LCC placement was larger than two.

Figure 4.5 shows measurements of the strain gauges attached to steel strip #5, installed on September 26, 2020. These strain gauges are labeled as top (T) or bottom (B), indicating the strain gauge location, increasing from 1 to 5 as the distance from the back facing of the wall panels increased. For example, strain gauge “5-T-1” means the strain gauge was on the top side in the front end of strip #5. Strip #1 was the uppermost strip, and strip #5 was the lowermost strip.

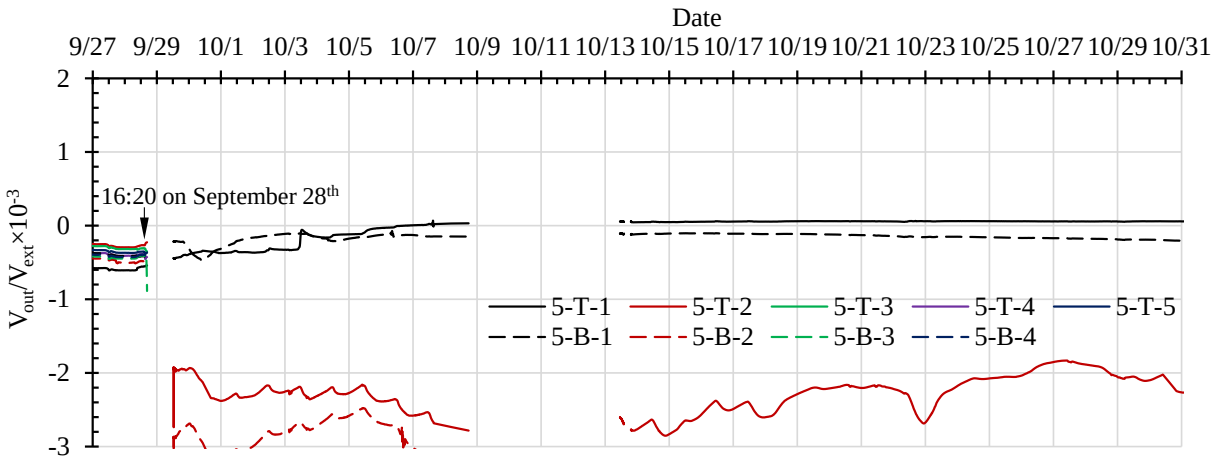

Figure 4.5: Readouts of Strain Gauges (Strip #5)

Except for the strain gauges near the back facing of the wall panels (5-T-1, 5-B-1, 5-T-2, and 5-B-2), the strain gauge measurements on strip #5 became larger than 2 $V_{out}/V_{exit}\times10^{-3}$ after 12:30 on September 29 (placement of the first LCC layer was finished at 15:40 on September 28). In addition, LCC temperatures near the wall panels were much lower than temperatures far from the wall panels, indicating that the high LCC temperatures may have damaged the strain gauges near the middle of the LCC mass, resulting in abnormal readings. Strain gauge damage also occurred on strips #1 through #4 (in the middle of the LCC mass); their readings were invalid because they exceeded 2 $V_{out}/V_{exit}\times10^{-3}$. Overall, almost all the strain gauges at locations 2–5 on the five strips displayed abnormal readings immediately following LCC placement, so only the readings of strain gauges near the wall panels (i.e., location 1) were considered valid.

Figure 4.6 shows changes of axial force and moment at the front ends of each strip (location 1) over time.

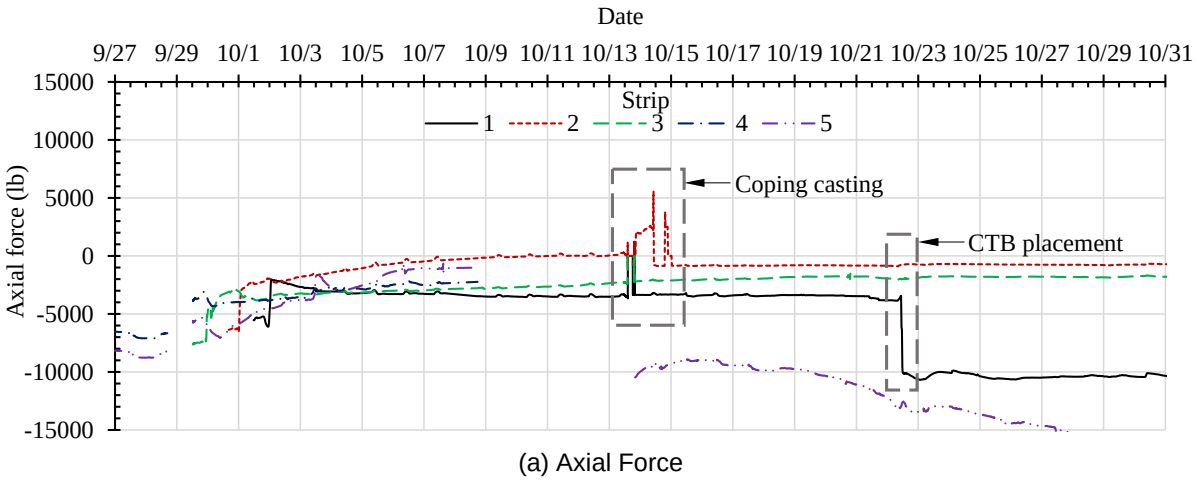

(a) Axial Force

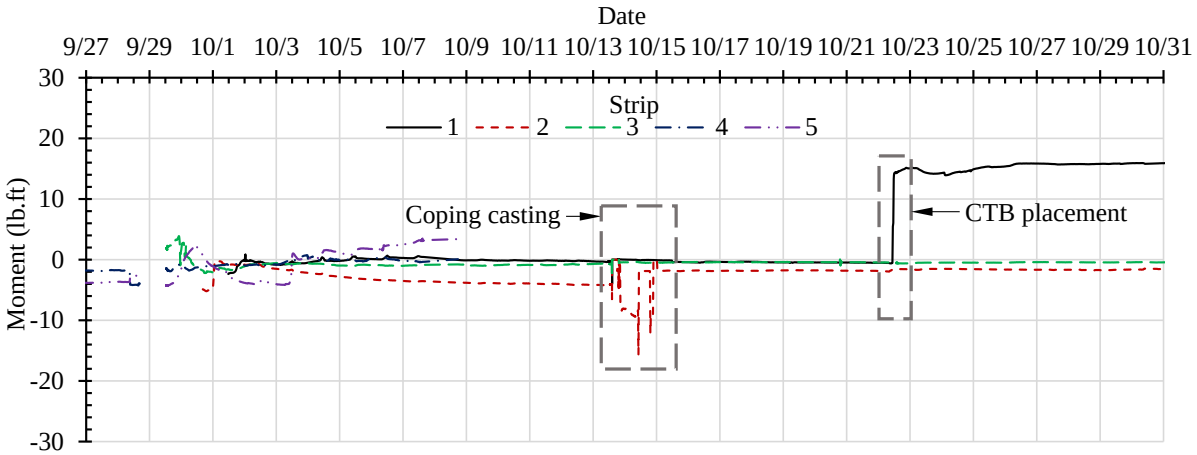

(b) Moment

Figure 4.6: Force and Moment at Front End of Strips

As shown in the figure, the force and moment at the front ends of strips #1 through #3 were approximately constant during LCC placement and for 4–6 hours after placement. After 11–16 hours, the force and moments of strips #1 through #3 changed gradually. Figure 4.6 also shows that casting of the coping changed the force and moment at the front ends of strips #1, #2, and #3, while placements of the CTB layer significantly changed the force and moment at the front end of strip #1. In addition, the axial force at the front ends of strips #1 and #2 varied slightly each day from October 4 to October 17 due to daily temperature changes. Overall, the moment at the front ends of all the strips was relatively small before October 31 (ranging from -20 lb·ft to 20 lb·ft).

4.3 Lateral Deformation and Settlement

The vertical shape array was removed before 10:00 on October 14, 2020, prior to casting of the coping. Figure 4.7 shows deformations of the vertical shape array directly behind the wall panels at 00:00 (midnight) relative to the position of the array at 00:00 on October 3 and temperatures measured by the vertical shape array at 0:00 on various dates. From October 3 to October 14, temperatures within elevations from -0.5 ft to 8.5 ft decreased over time at a decreasing rate. After October 5, however, temperatures behind the wall panels increased from the -0.5 ft elevation to 5.25–5.90 ft elevations and then decreased with additional elevation. Due to temperature reduction over time starting on October 3, LCC contraction caused movements of the vertical shape array away from the wall panels, as shown in Figure 4.7.

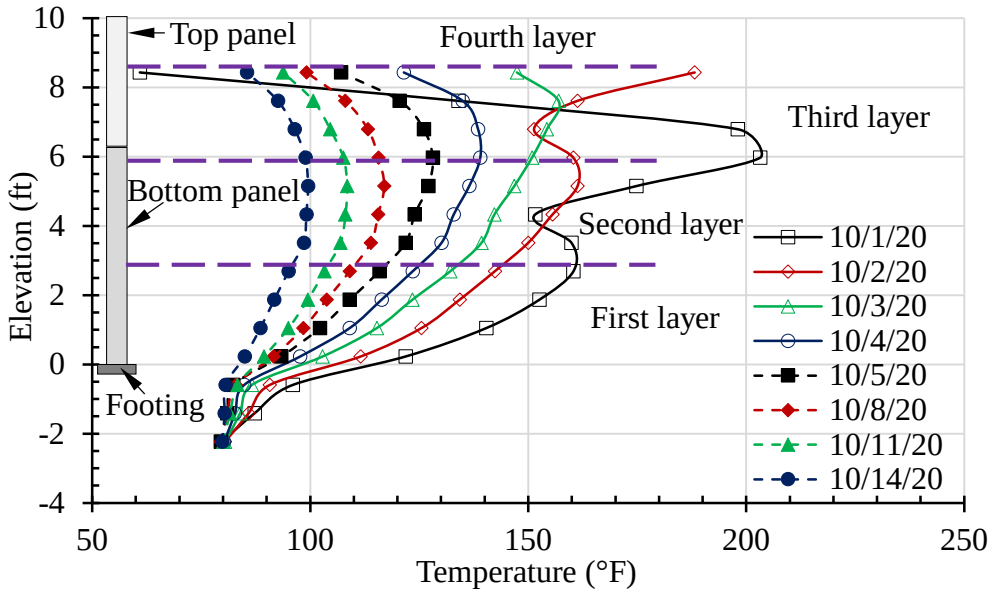

(a) Temperature Right Behind Wall Facing

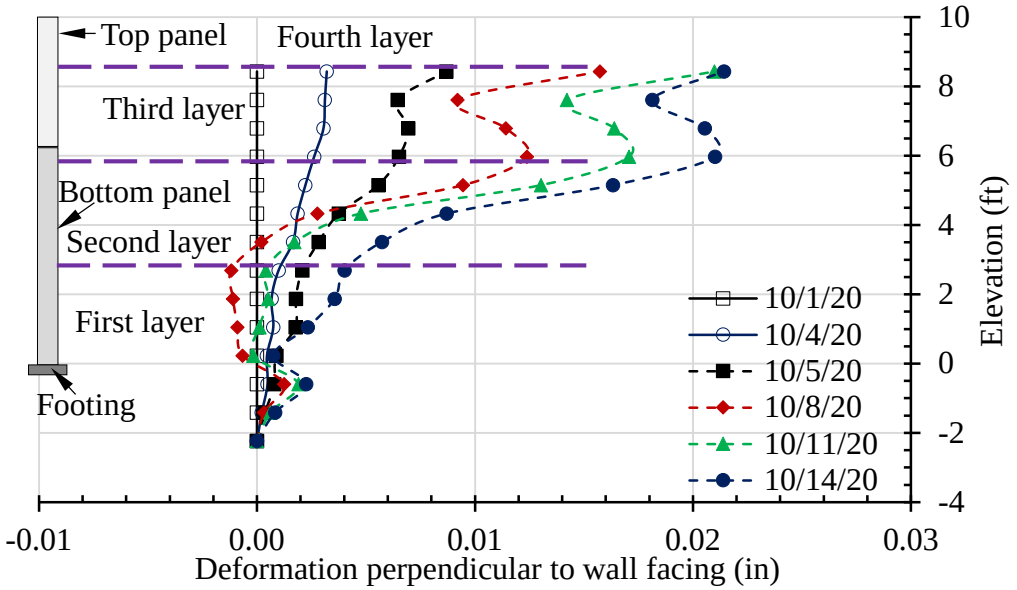

(b) Displacements Perpendicular to Wall Facing

Figure 4.7: Temperature and Displacement Measured by Vertical Shape Array

Figure 4.8 shows settlements of LCC at the base of the backfill at 00:00 relative to the position of the shape array between 11:00 and 12:00 on September 28, 2020, and the temperatures at 0:00 on various dates. Settlements were negligible during the first month after casting, with a

maximum recorded value of less than 0.18 in., which was likely a function of the positioning of the shape array in the PVC pipe, given the shape of the curve in Figure 4.8(b).

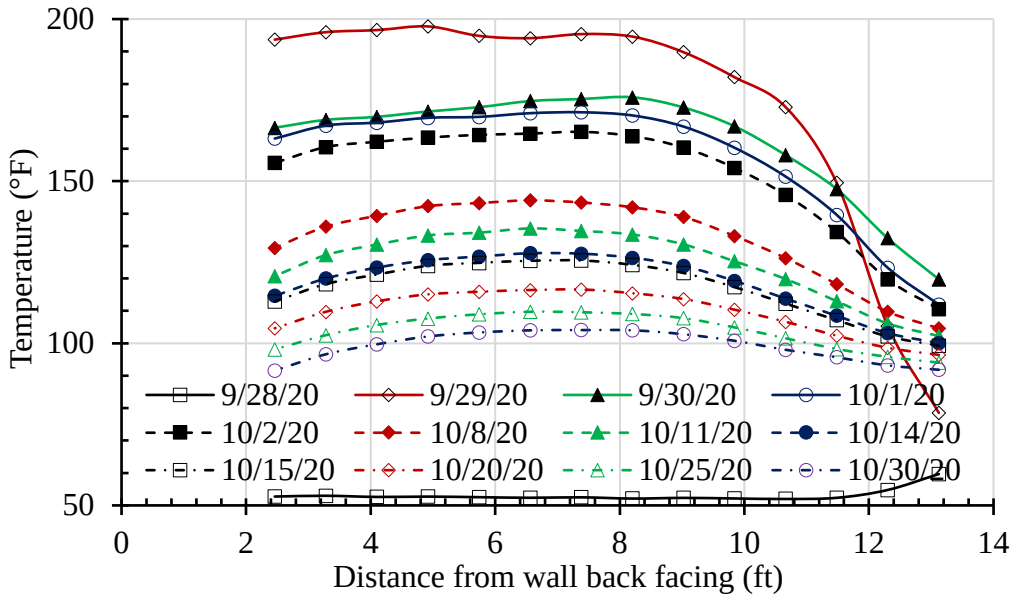

(a) Temperatures at the Base of LCC Backfill

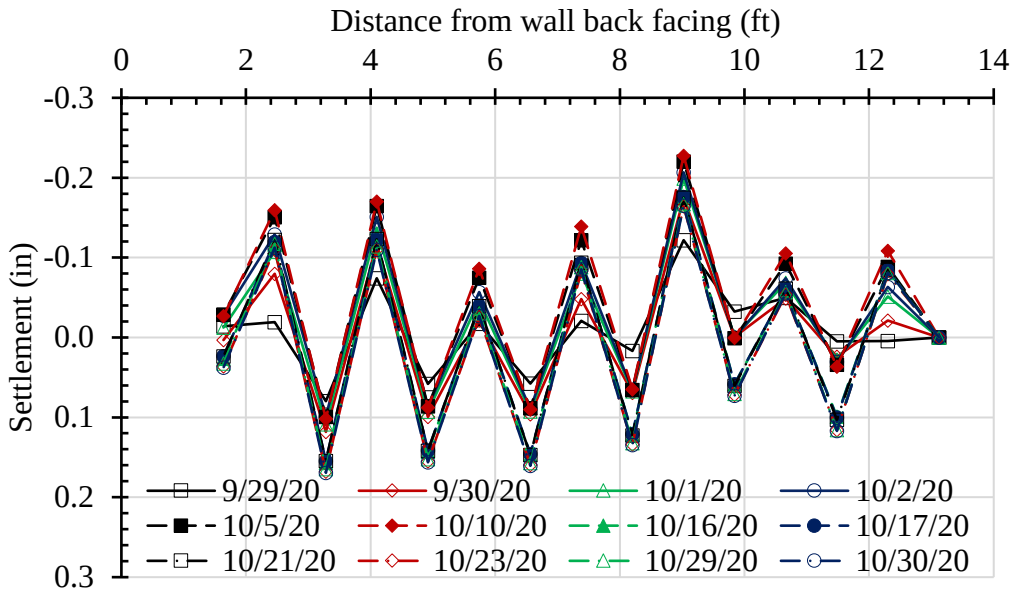

(b) Settlements at the Base of LCC Backfill

Figure 4.8: Temperature and Settlement Measured by Horizontal Shape Array

As shown in the figure, on September 29 the temperatures near the slope of the retained soil were much lower than the temperatures far from the slope, with a decreasing difference over time. Because the end of the horizontal shape array far from the wall back facing was cast into a concrete block before LCC placement, the temperature increase at this end was minor due to thermal insulation of the concrete. In addition, the temperature in the first LCC layer decreased rapidly from September 29 to September 30 because heat emitted from the newly placed LCC lifts did not significantly increase the temperature in the first LCC layer due to continual heat loss from the first layer to the ground and the low heat conductivity of LCC. Additionally, the cement hydration rate of LCC decreased gradually over time after reaching its peak value (i.e., heat emitted in the first LCC lift decreased gradually over time), as shown in Figure 4.8(a). Therefore, the temperature reductions measured by the horizontal shape array were not significant from September 30 to October 2. The temperature decreased over time at a decreasing rate from October 5 to October 30 due to a decreasing cement hydration rate. Placement of the cushion layer on October 16 and the CTB layer on October 21 and 22 did not result in significant settlement increases, as shown in Figure 4.8(b). Since the excavated portion of the original ground was backfilled on October 29, a comparison of settlements between October 29 and October 30 indicated that the effects of the backfilling process in front of the wall panels on the ground settlements were negligible.

4.4 Conclusions

Results of this study showed that, during the setting time of a newly placed LCC layer (typically 2–4 hours after LCC placement), the LCC applied hydraulic pressure to the back facing of the MSE wall panels. In addition, the temperature in a newly placed LCC layer reached its peak value 12–16 hours after the LCC layer was placed, and then the temperature decreased gradually over time. The peak temperature for this test section exceeded 200 °F in some locations. Newly placed LCC layers had a limited effect on the temperature in the underlying layer due to the slow transmission and dispersal of heat from the base of the fill. Daily temperature variations in LCC directly behind the wall panels lagged daily variations of air temperature during LCC curing. As a

result, LCC expansion behind wall panels at high temperatures could increase lateral earth pressures behind wall panels.

Results also showed that contraction of LCC backfill with temperature reductions potentially redistributed vertical pressures on the ground, increasing vertical pressure in the middle of the base but decreasing vertical pressures near the wall panels and the retained soil. Heat emitted from cement hydration increased LCC temperature significantly, potentially damaging foil strain gauges. Certain construction activities, specifically placement of cushion and CTB layers, could change the axial forces and moments at the front ends of the strips in LCC-MSE walls. In addition, daily variations of air temperature may result in small daily variations of axial forces and moments at the front ends of the strips. Lateral deformations in the short-term were small, with a maximum value of approximately 0.02 from day 3 to day 13. Vertical deformations were negligible during the first month after construction.

Chapter 5: MSE Wall Performance

This chapter contains an analysis of one year of field-monitoring data from November 2020 to November 2021. The data included vertical earth pressures and temperatures at the base of the LCC backfill, lateral earth pressures and temperatures at the wall back facing, LCC settlements, and wall facing settlements.

5.1 Vertical and Lateral Earth Pressures

PCCP was placed on December 2, 2020, of this study. Figure 5.1 shows the effects of PCCP placement on vertical earth pressures at the base of the LCC backfill and lateral earth pressures behind the back of the wall facing. Vertical and lateral earth pressures were averaged on December 1 and December 3, and the air temperatures on these days were 35.78 and 35.24 °F, respectively, meaning the effects of LCC expansion and contraction due to air temperature difference were negligible.

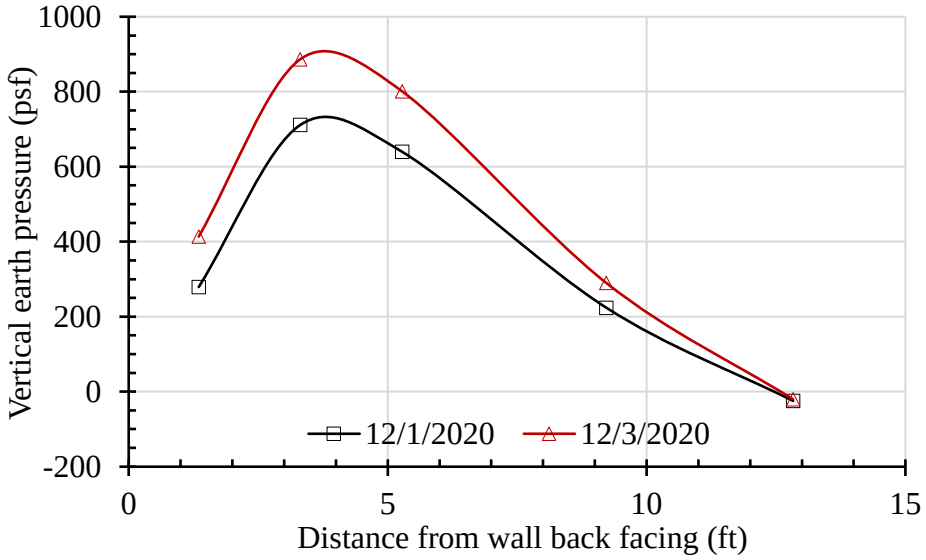

(a) Vertical Earth pressures

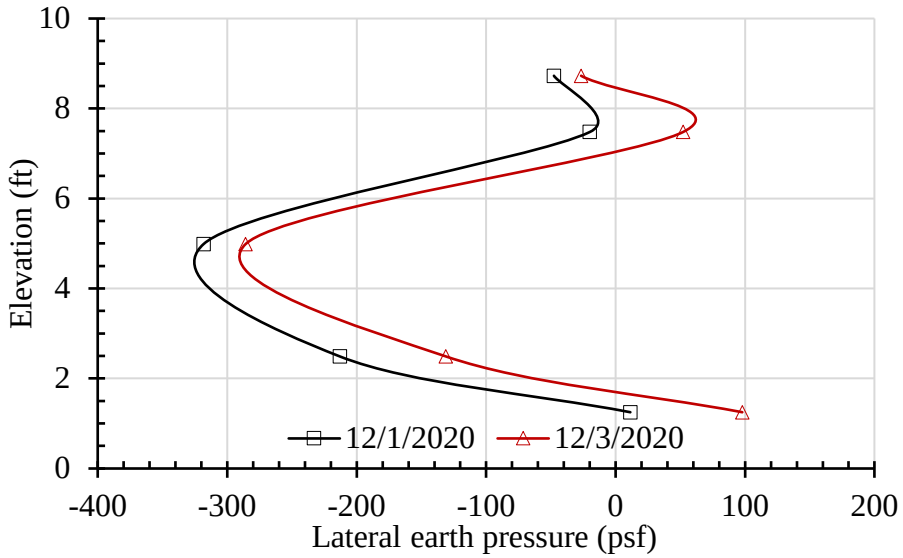

(b) Lateral Earth Pressures

Figure 5.1: Effects of PCCP Layer Placement on Vertical and Lateral Earth Pressures

Figure 5.1(a) shows that the vertical earth pressures measured by EPC-01, EPC-02, EPC-03, EPC-04, and EPC-05 increased by 4.5, 66.1, 161.1, 175.1, and 134.5 psf, respectively, from December 1 to December 3. Since the thickness of the placed PCCP layer was 1.0 ft and the typical unit weight of concrete is 144 pcf, the PCCP layer applied a uniform pressure of 144 psf on the

top of the CTB layer. The increases in vertical earth pressure generally matched the weight of the PCCP layer. In addition, more weight from the pavement was transferred to EPC-03 and EPC-04 (near the wall facing), while less weight was transferred to EPC-01 and EPC-02 (far from the wall facing). Figure 5.1(b) shows that the lateral earth pressures measured by EPC-06, EPC-07, EPC-08, EPC-09, and EPC-10 increased by 86.6, 82.0, 32.5, 72.1, and 21.1 psf, respectively, from December 1 to December 3. The average lateral earth pressure increase for these five earth pressures was 58.9 psf, and the average vertical earth pressure near the wall facing (EPC-03, EPC-04, EPC-05) was 156.9 psf, so a lateral earth pressure coefficient of 0.38 was adopted for the LCC.

Figure 5.2 shows measured vertical earth pressures at the base of the LCC backfill and measured lateral earth pressures behind the wall facing from November 2020 to November 2021.

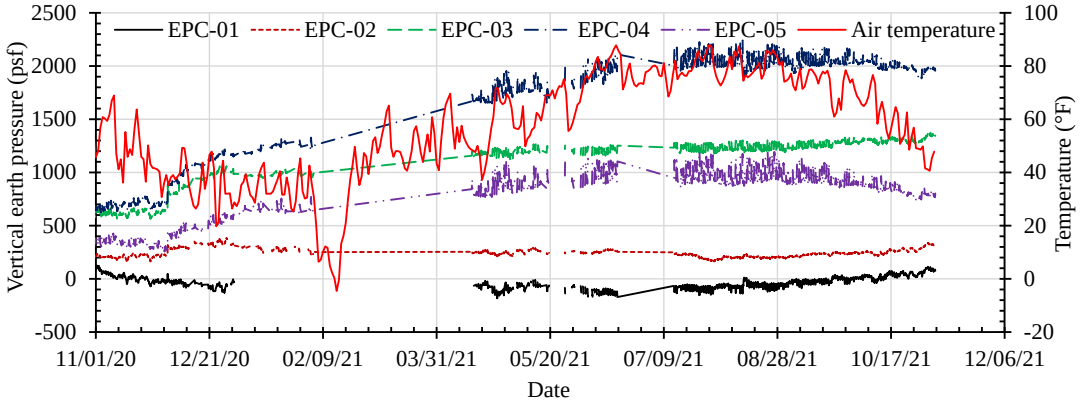

(a) Vertical Pressure at the Base of LCC

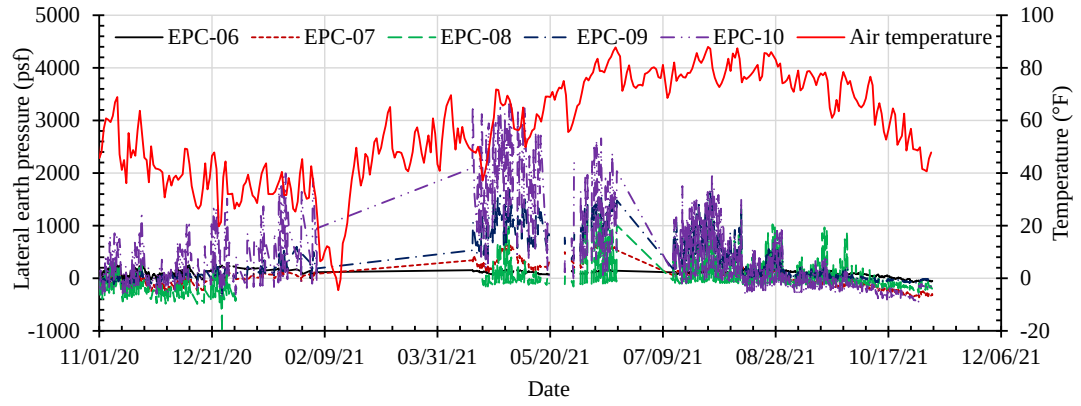

(b) Lateral Earth Pressure Behind Wall Back Facing

Figure 5.2: Vertical and Lateral Earth Pressures (November 2020 to November 2021)

After the placement of the PCCP layer, pressure readings of EPC-01 decreased while pressure readings of EPC-03, EPC-04, and EPC-05 increased until February 2021, potentially due to the gradual shifting of the retained soil behind the LCC, which applied increasing lateral pressure to the back of the LCC. The LCC tended to rotate about the toe of LCC-MSE wall, resulting in increasing pressures at the base of the LCC near the wall facing but decreasing pressures far from the wall facing over time. Another cause of the change in vertical pressures may have been the redistribution of LCC weight due to changes of temperature distribution in the LCC. As temperature distribution changed in the LCC, the LCC weight that was transferred to the wall facing via the LCC and wall facing panels and/or through strip reinforcements varied. After April 2021, however, vertical earth pressures measured by EPC-04 and EPC-05 changed with air temperature in the same trend (i.e., vertical earth pressures increased as air temperature increased and decreased as air temperature decreased). Furthermore, daily air temperature variations redistributed the weight of the backfill material, thereby inducing daily vertical pressure variations. Figure 5.2(b) also shows that daily air temperature variations caused daily, occasionally substantial, variations of lateral earth pressures behind the back of the wall facing.

Figure 5.3 shows vertical earth pressure variations by distance from the back of the wall facing and lateral earth pressure variations by wall elevation from July 13 to November 5, 2021. Figure 5.3 also shows the minimum, average, and maximum measured earth pressures during this period.

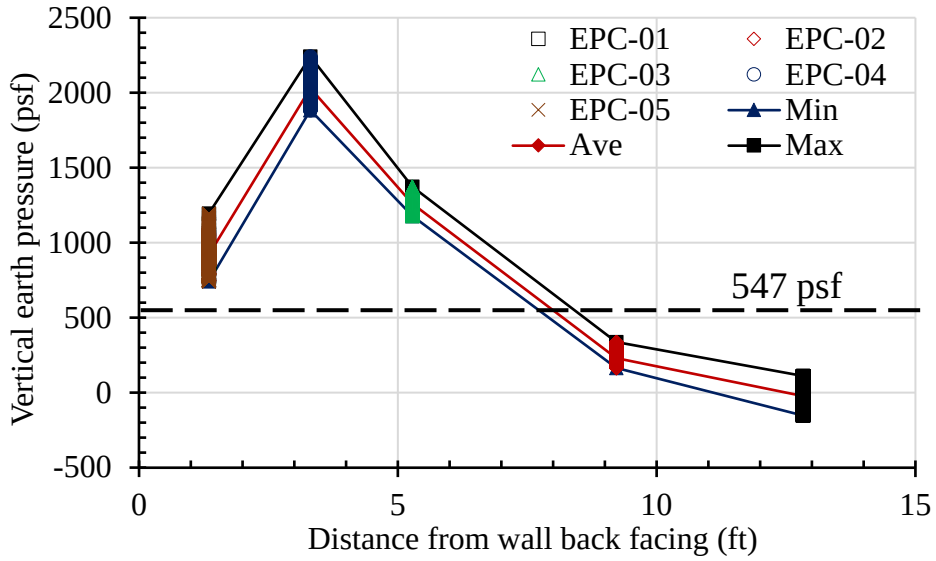

(a) Vertical Earth Pressures with the Distance from Wall Back Facing

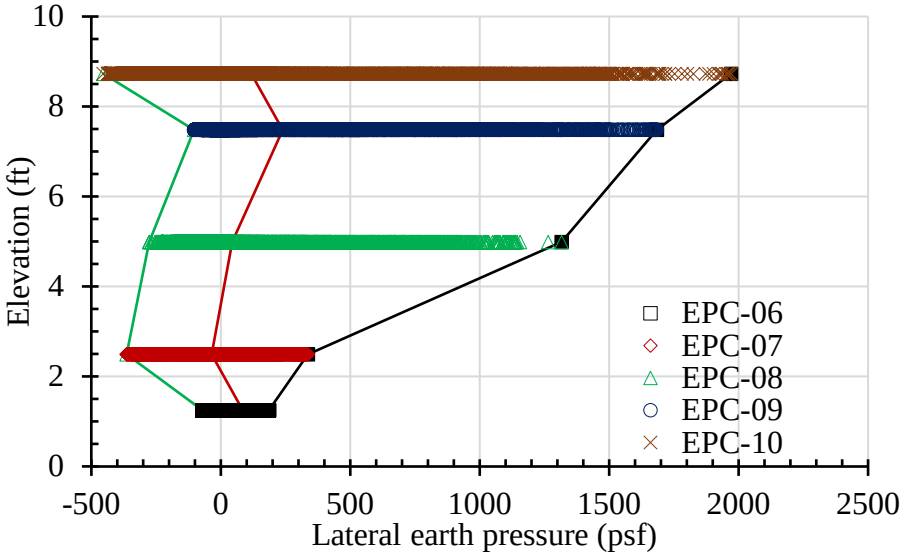

(b) Lateral Earth Pressure with the Elevation

Figure 5.3: Variations of Vertical and Lateral Earth Pressures

The average elevation of EPC-01 to EPC-05 was 4 inches below the top of the leveling pad, so the weight of the LCC (10.2 ft thick, ρ = 32 pcf), cushion layer (4 inches thick, ρ = 115 pcf), CTB layer (4 inches thick, ρ = 115 pcf), and PCCP layer (1.0 ft thick, ρ = 144 pcf) was applied to those five cells. Theoretically, the vertical earth pressure on all the cells was 547 psf (10.2×32+1/3×115+1/3×115+1×144=547pcf). Figure 5.3(a) shows that the vertical earth pressures

measured by EPC-01 and EPC-02 were less than the theoretical earth pressure, but the vertical earth pressures measured by EPC-03, EPC-04, and EPC-05 were more than the theoretical earth pressure. Variations of the measured lateral earth pressures were much larger than the measured vertical earth pressures, and variations of lateral earth pressures became larger as the elevation increased, as shown in Figure 5.3(b). The maximum lateral earth pressure was 239 psf at the elevation of 1.25 ft, but the maximum lateral earth pressure reached 1,970 psf at the elevation of 8.73 ft, which was more than eight times 239 psf.

Figure 5.4 shows the average vertical and lateral earth pressures and average air temperature per week from November 2020 to November 2021.

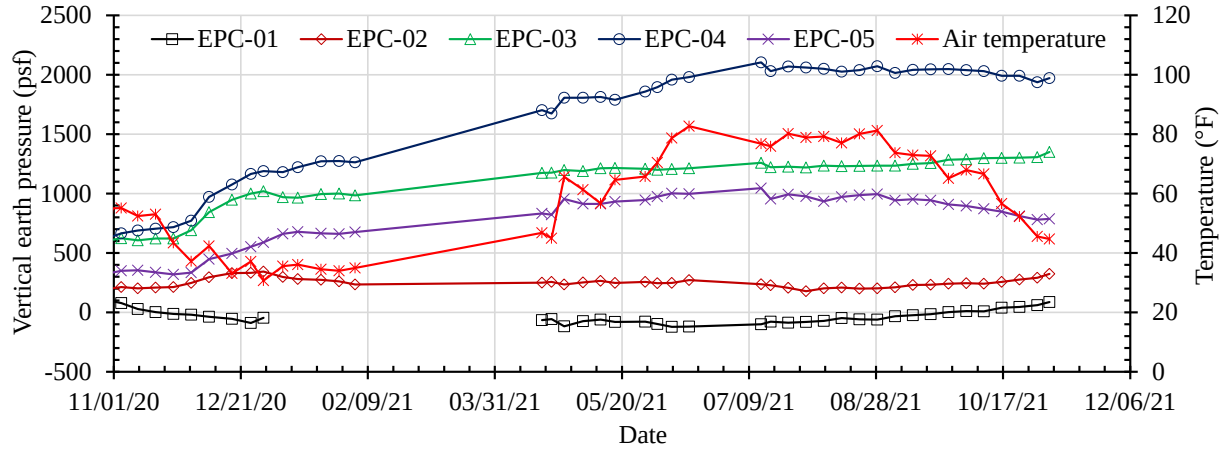

(a) Average Vertical Earth Pressure

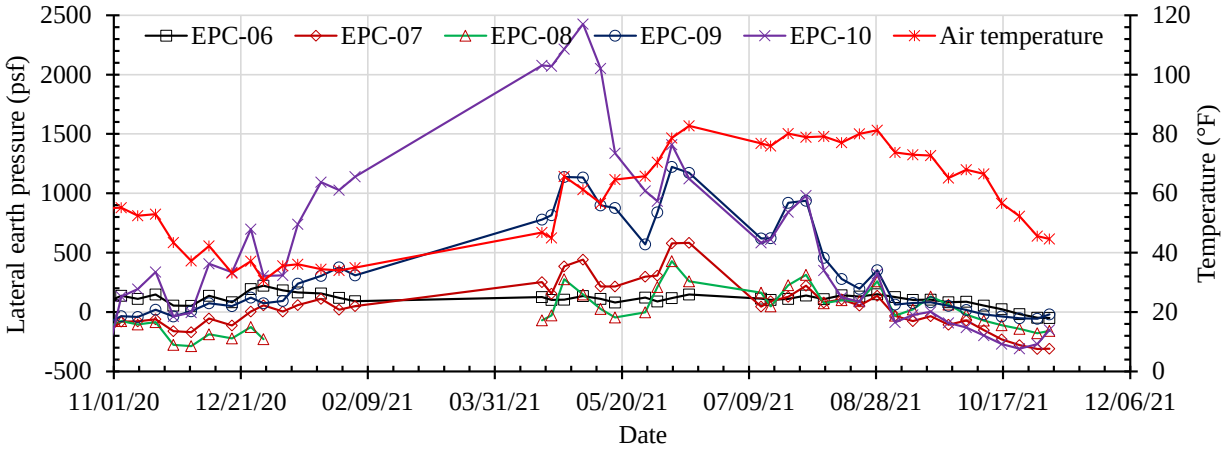

(b) Average Lateral Earth Pressure

Figure 5.4: Average Vertical and Lateral Earth Pressures

Figure 5.4(a) shows that vertical earth pressure variations were not significant for EPC-01 to EPC-05, especially from July to November 2021. In general, vertical earth pressures measured by EPC-01 and EPC-02 decreased as air temperature increased, while vertical earth pressures measured by EPC-04 and EPC-05 increased as air temperature increased. Figure 5.4(b) shows that measured lateral earth pressures were highly correlated with air temperatures, especially for EPC-08, EPC-09, and EPC-10. In general, high air temperatures induced high lateral earth pressures. Since EPC-06 had the lowest elevation among EPC-06 to EPC-10, and the excavation in front of the wall facing was backfilled on October 29, 2020, air temperature had a limited effect on the pressure readings. Due to low air temperatures beginning in mid-October, LCC backfill did not exert any lateral earth pressures on the wall facing. For EPC-10, the average pressure May 1–7, 2021, was 2,426 psf, followed by a decreasing average pressure.

The vertical spacing between the top two strips was 1.25 ft, and the top strip was 1.5 ft from the LCC surface. Since the horizontal spacing of the strips was 2.2 ft, the peak lateral pressures for an area with a length of 2.2 ft and height of 2.1 ft should be carried by the top strip. Therefore, the force at the front end of the top strip was approximately 11,200 lb. Small panel movement under this level of force potentially caused this stress reduction, and shifting of the panel may have induced corresponding drops of lateral earth pressures measured by EPC-08 and EPC-09, as shown in Figure 5.4(b).

Figure 5.5 illustrates the relationships between average vertical or lateral earth pressures and average air temperatures per week for July 14, 2021, to November 5, 2021, long after hydration was complete.

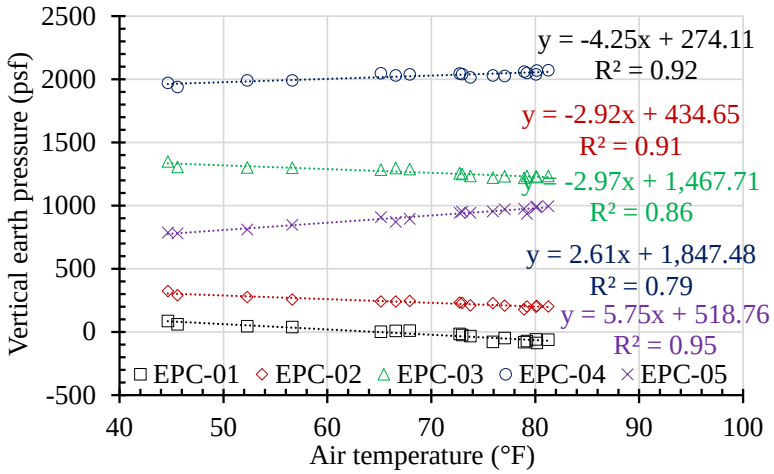

(a) Relationship Between Average Vertical Earth Pressures and Air Temperatures

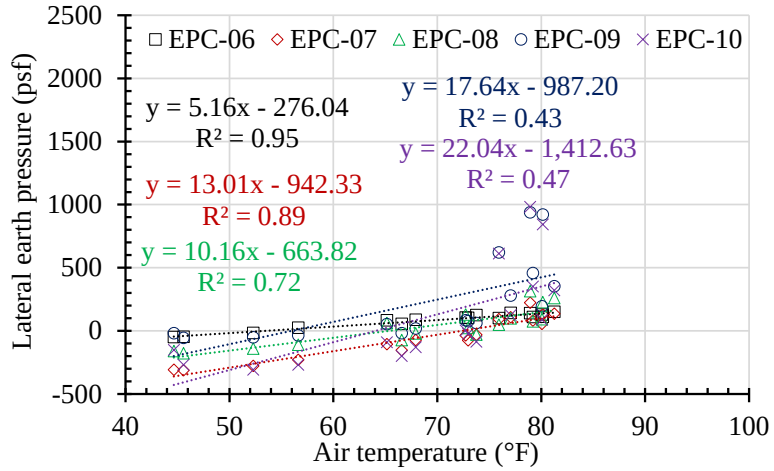

(b) Relationship Between Average Lateral Earth Pressures and Air Temperatures

Figure 5.5: (a) Relationship between Average Vertical and Lateral Earth Pressures and (b) Air Temperature

As shown in Figure 5.5(a), increased air temperature resulted in increased vertical pressures for EPC-04 and EPC-05 but decreased vertical pressures for EPC-01, EPC-02, and EPC-03. In general, the temperature changes caused limited vertical earth pressure changes. As the temperature increased by 20 °F, vertical earth pressure measured by EPC-01 decreased by 85 psf and vertical earth pressure measured by EPC-05 increased by 115 psf. Air temperature changes caused significant changes to lateral earth pressures. As the temperature increased by 20 °F, lateral earth pressure measured by EPC-06 decreased by 103 psf and lateral earth pressure measured by EPC-10 increased by 441 psf. In general, high air temperature resulted in high lateral earth pressures, as shown in Figure 5.5(b).

During the period of July to November 2021, September 26 had the highest daily air temperature variation (33 °F). Figure 5.6 shows temperatures and vertical earth pressures at the base of the LCC, and Figure 5.7 shows temperature and lateral earth pressures behind the wall facing at 0:00, 04:00, 08:00, 12:00, 16:00, and 20:00 on September 26, 2021.

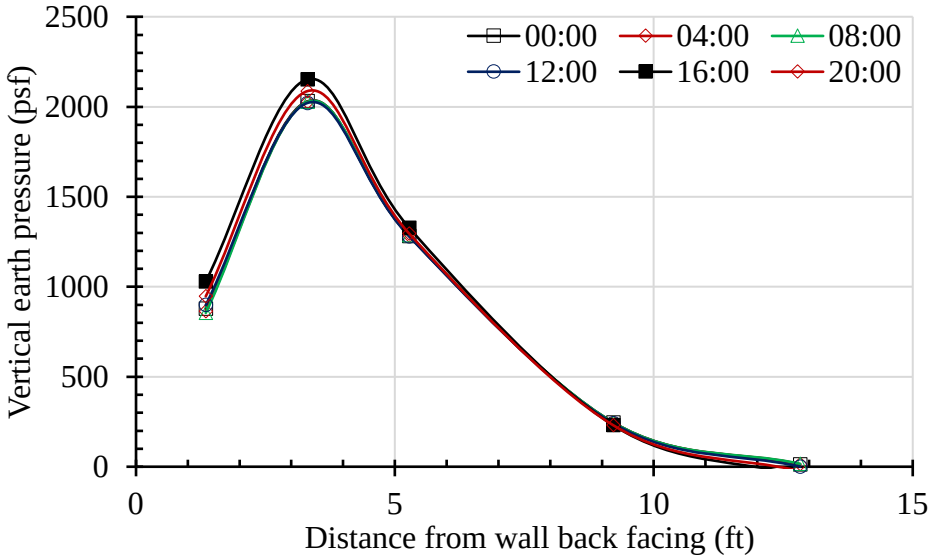

(a) Effects of Daily Air Temperature on Temperatures at the Base of LCC

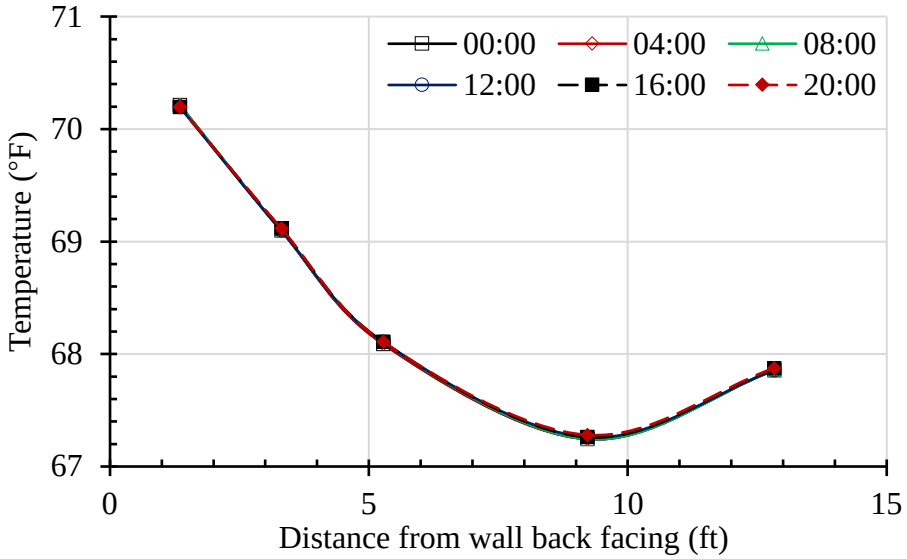

(b) Effects of Daily Air Temperature on Vertical Earth Pressures at the Base of LCC

Figure 5.6: Effects of Daily Air Temperature on (a) Temperatures and (b) Vertical Earth Pressures at LCC base

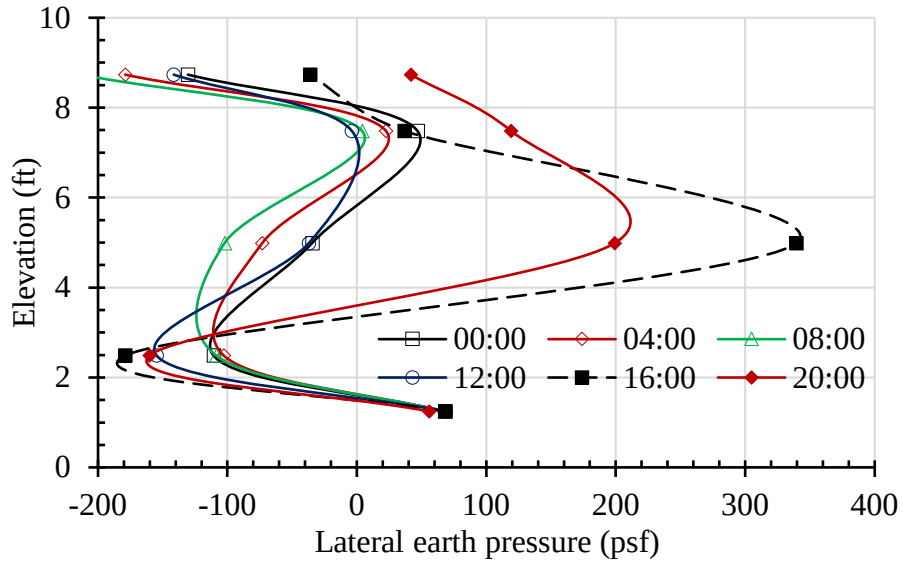

(a) Effects of Daily Air Temperature on Temperatures Behind the Wall Facing

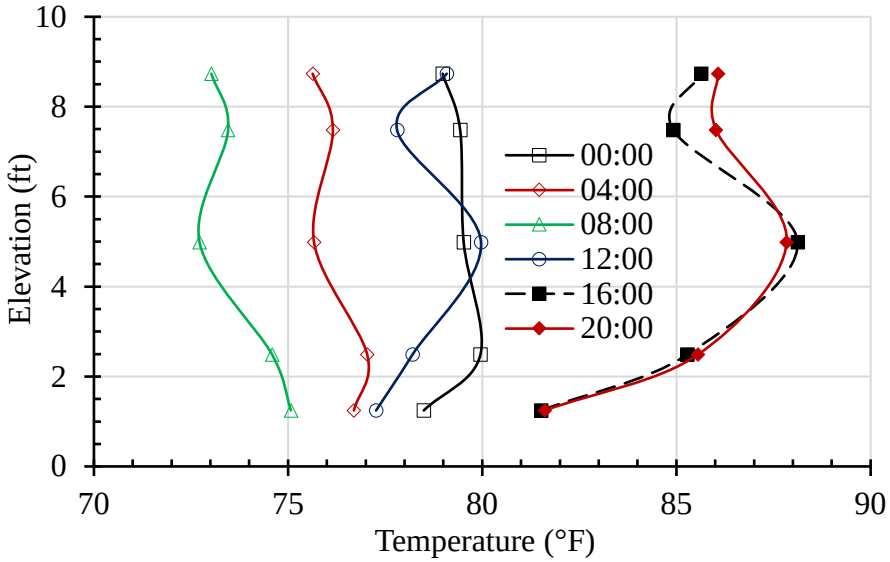

(b) Effects of Daily Air Temperature on Lateral Earth Pressure Behind Wall Back Facing

Figure 5.7: Effects of Daily Air Temperature on (a) Temperatures and (b) Lateral Earth Pressures behind Wall Facing

Figure 5.6 shows that daily air temperatures had a negligible effect on the temperature at the base of the LCC and a modest effect on vertical earth pressures at the base of the LCC. Figure 5.7 shows that, from 0:00 to 08:00, the daily temperature behind the wall facing decreased and then increased until 16:00, followed by approximately constant temperature until 20:00. At the elevation of 1.25 ft (EPC-06), daily air temperature variation had a modest effect on the lateral

earth pressure but a significant effect on lateral earth pressures at elevations of 5.0 (EPC-08), 7.5 (EPC-09), and 8.7 ft (EPC-10), with a maximum change of approximately 350 psf.

From July 14 to November 5, 2021, the highest daily air temperature was 88.0 °F on July 29, while the lowest daily air temperature was 40.6 °F on November 3. Figure 5.8 shows earth pressures and temperatures at 0:00 on these two days.

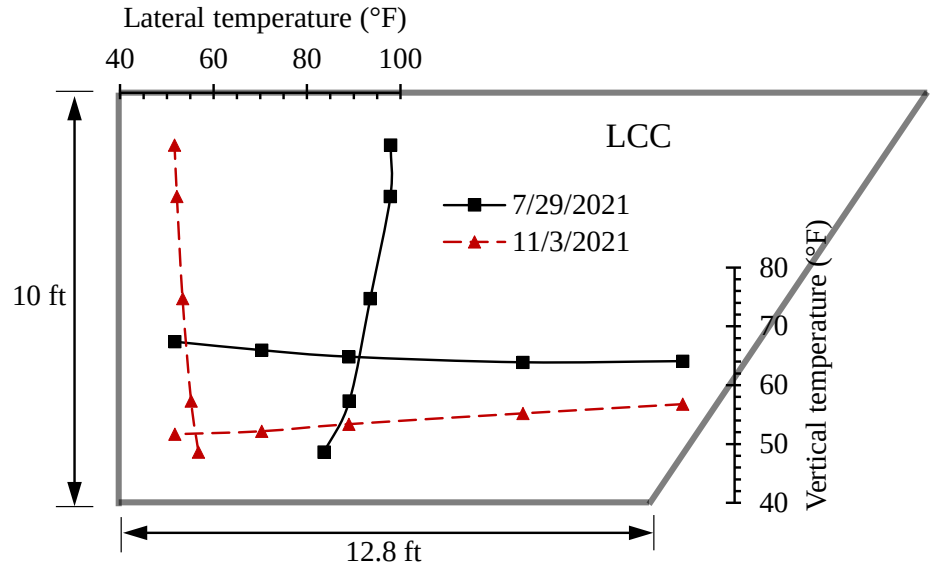

(a) Temperatures

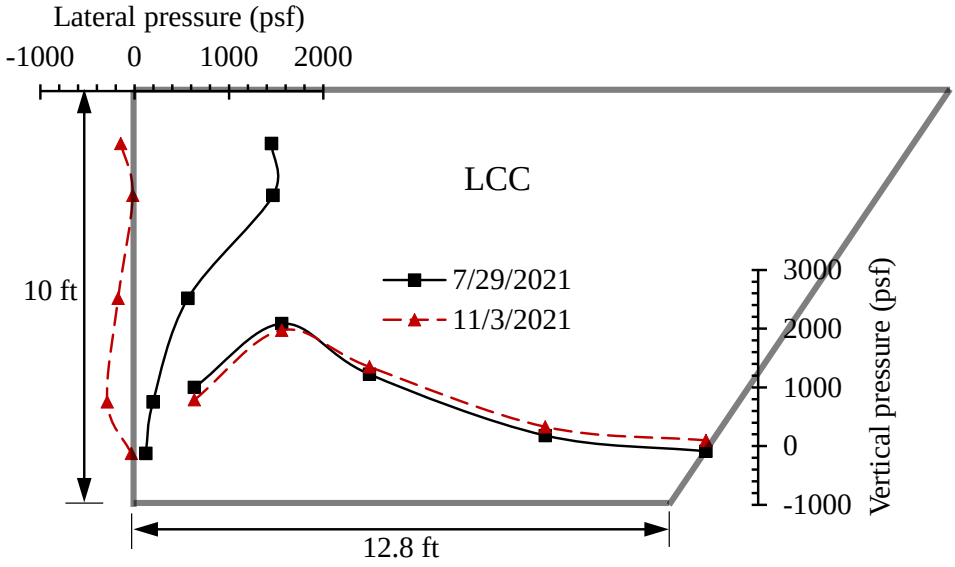

(b) Vertical and Lateral Earth Pressures

Figure 5.8: (a) Temperatures and (b) Pressures at 0:00 on July 29 and November 3, 2021

Since the wall facing and the top surface of the LCC were exposed to air temperature and solar radiation, heat transferred from the top left to the bottom right at high air temperature (July 29, 2021) and from the bottom right to the top left at low temperature (November 3, 2021). Therefore, temperatures behind the wall facing increased as the elevation increased, and the temperature at the base of the LCC decreased as the distance from the wall facing increased on July 29, 2021, as shown in Figure 5.8(a). Figure 5.8(b) shows that vertical earth pressures decreased near the wall facing but increased far from the wall facing on July 29 compared to data from November 3. In addition, lateral earth pressures behind the wall facing decreased on November 3 compared to July 29; the lateral earth pressure reduction from July 29 to November 3 increased as the elevation increased. The difference of lateral earth pressures between these two days and the magnitude of the larger lateral earth pressure values indicate that lateral earth pressures induced by air temperature changes should be considered when designing LCC-MSE walls.

5.2 LCC and Wall Facing Settlements

Figure 5.9 shows temperatures and settlements (11:00–12:00 on September 28, 2020) measured by the shape array at distances of 3.28, 6.56, and 9.84 ft from the wall facing. Figure 5.9 shows that placement of the PCCP layer on December 2, 2020, induced minimal additional settlement, while Figure 5.10 shows settlements measured by the shape array before LCC placement. Since the LCC during placement was in slurry form, placement of the first LCC lift caused repositioning of the horizontal shape array, which may have caused the wavy settlement curves in Figure 5.10. The slight settlement increase from November 15, 2020, to January 17, 2021, was caused by the PCCP placement, while the settlement increase from February 3 to June 10, 2021, may have been induced by traffic loading or consolidation of the ground soil.

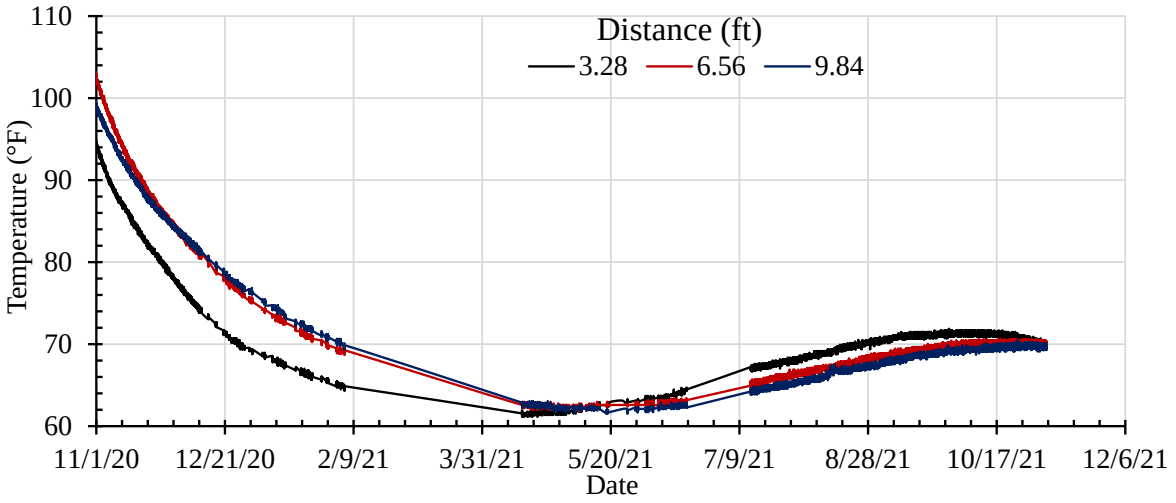

(a) Temperatures

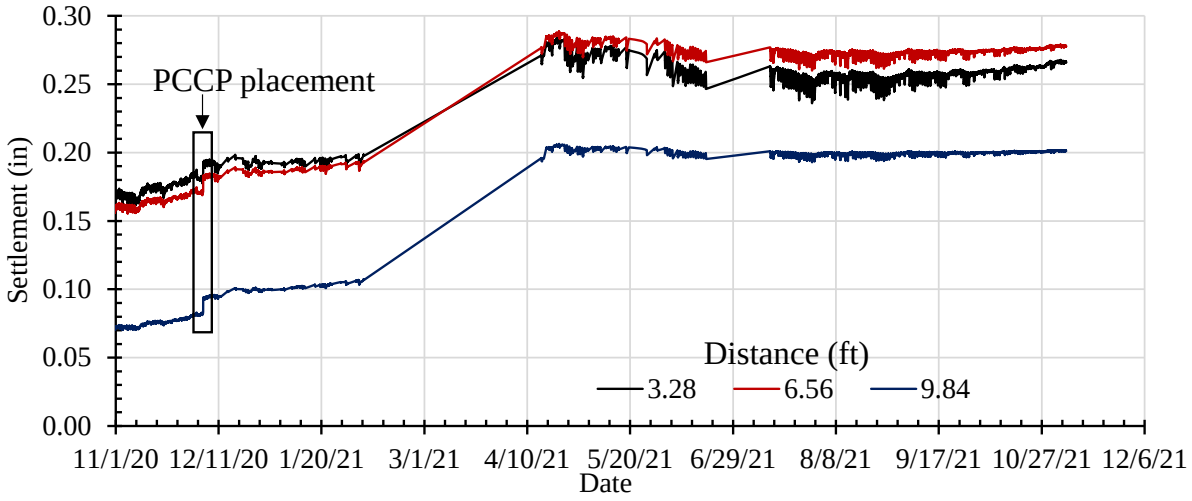

(b) Settlements

Figure 5.9: (a) Temperatures and (b) Settlements of LCC Measured by Shape Array

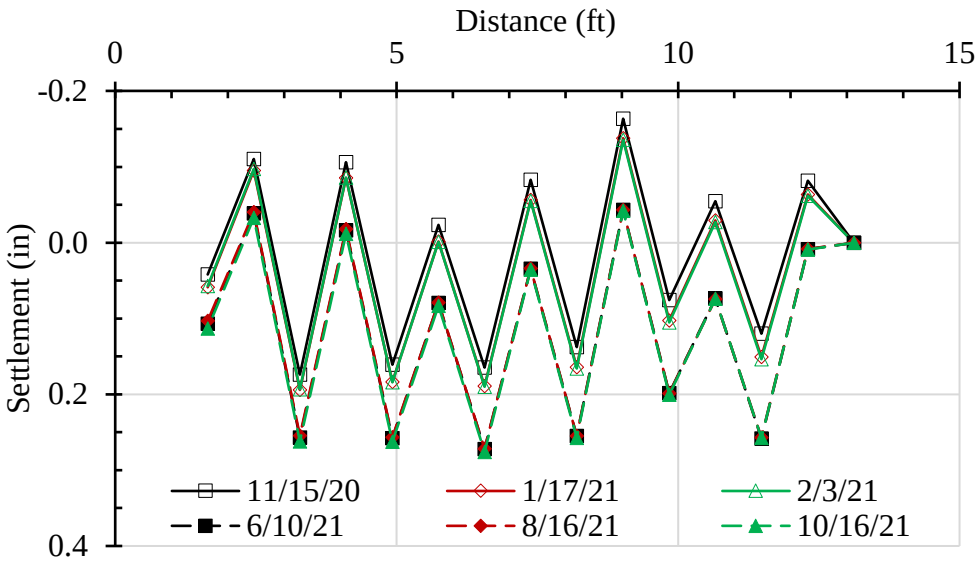

Figure 5.10: Settlements of LCC Measured by Shape Array

Survey targets A, B, H, I, and J were installed on September 8, 2020, while survey targets C, D, E, F, and G were installed on September 17, 2020. Prior to September 8, backfilling of the AG-MSE wall adjacent to the LCC-MSE wall segment was almost finished. In addition, only the bottom wall facing panels for the LCC-MSE segment were constructed before September 17, 2020. The top wall facing panels were placed during LCC placements, meaning placement of the upper wall facing panels could have caused the survey targets for the LCC-MSE wall to move, creating difficulties when comparing total settlements and deformations of wall facings of the AG-MSE and LCC-MSE walls. On average, however, results measured by the total station after October 15, 2020, showed that the LCC-MSE wall settled less than the AG-MSE wall by 0.04 inches (December 5, 2020), 0.06 inches (June 18, 2021), and 0.13 inches (August 25, 2021). Figure 5.11 shows wall facing deformations and settlements measured by survey targets immediately after their installation in the LCC-MSE wall. When the survey targets moved outward or downward, the measured deformations and settlements were positive in Figure 5.11.

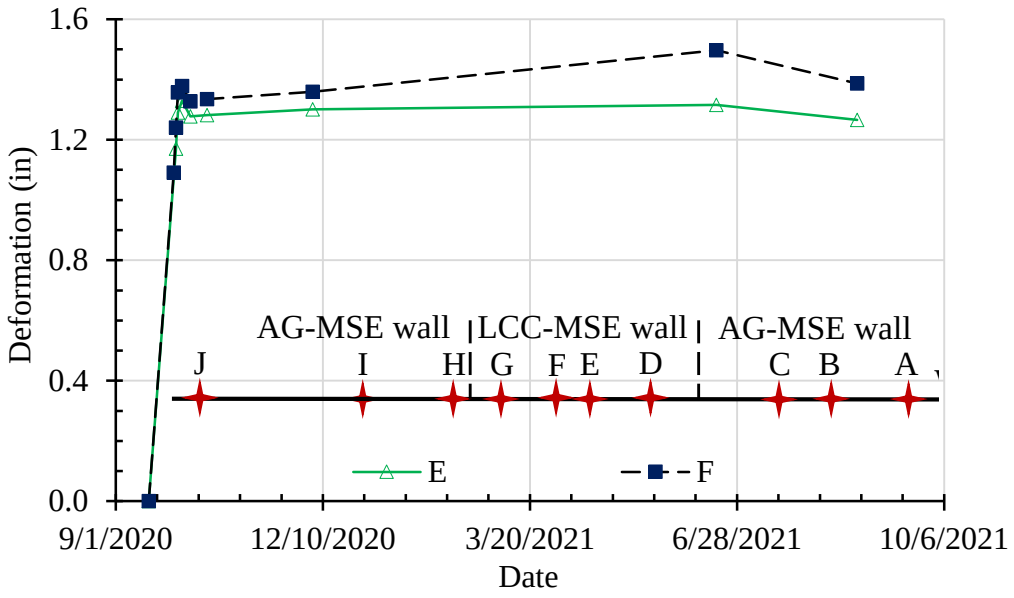

(a) Deformation of Wall Facing

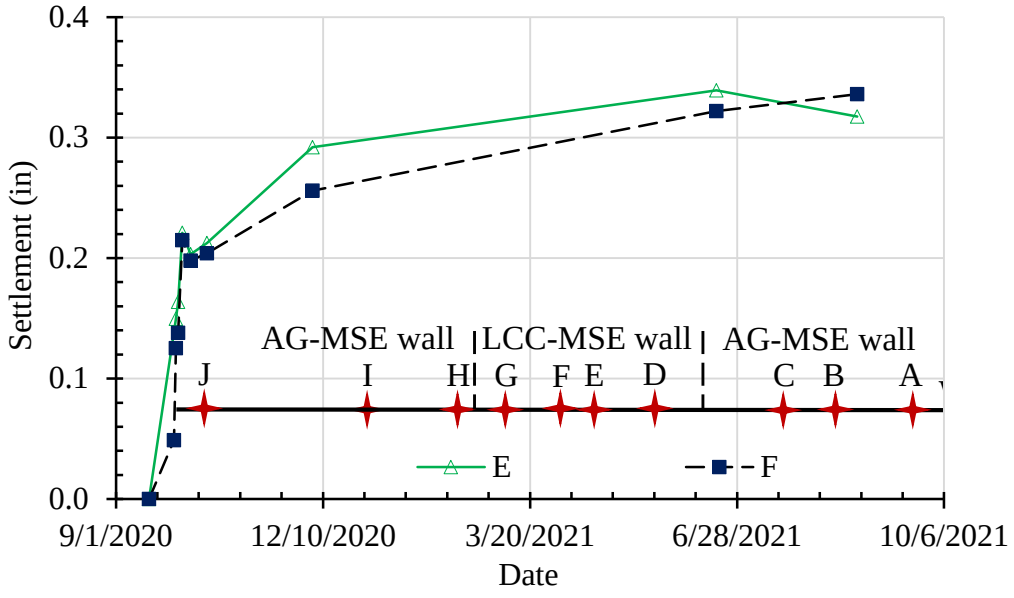

(b) Settlement of Wall Facing

Figure 5.11: (a) Deformations and (b) Settlements of Wall Facing

Measured settlements were small, with a total settlement of approximately 0.35 inches in the initial measurements and approximately 0.1 inches after construction was complete. Although measured lateral deformations exceeded 1.5 in., most of the deformations occurred during construction, likely when the liquid LCC flowed against the panels during placement and caused

movement. Lateral movement during this phase could be avoided by more rigid bracing. Essentially, no lateral creep was observed after the wall was complete.

5.3 Temperature Changes

Figure 5.12 shows air temperatures and temperatures measured by EPCs at the base of the LCC and thermistors from November 1, 2020, to November 5, 2021. Due to malfunctions of the dataloggers, some data from February 5 to April 14, 2021, and from June 18 to July 13, 2021, were not recorded.

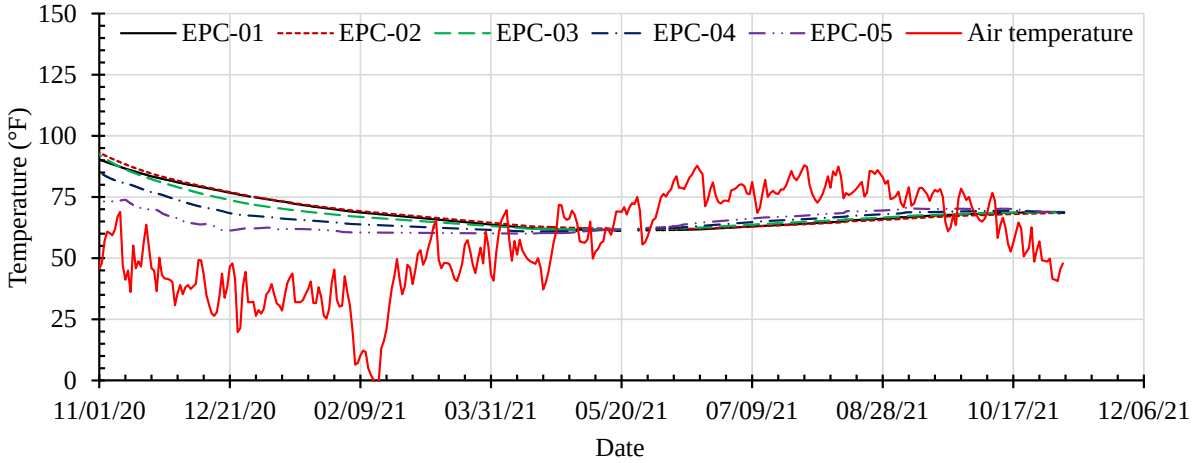

(a) At the Base of LCC Backfill

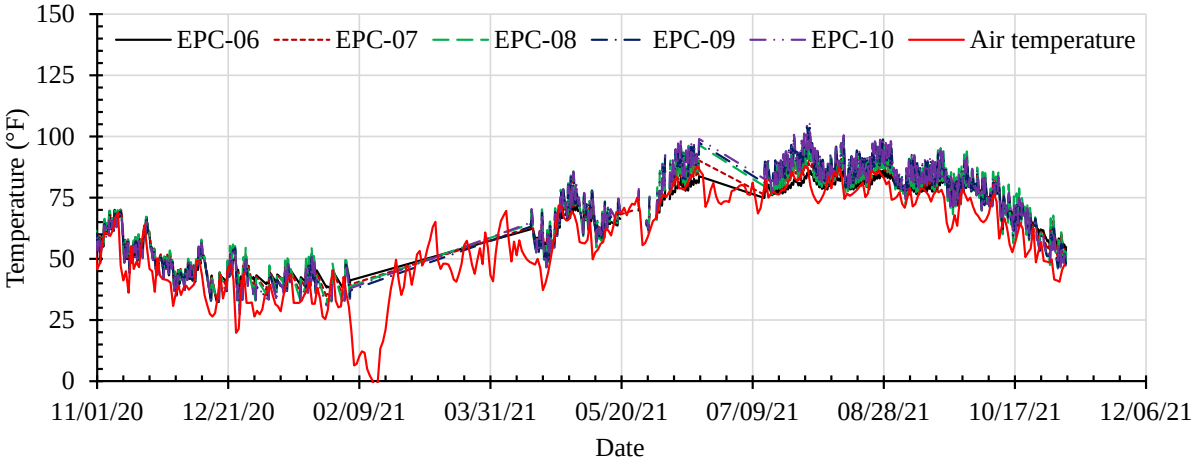

(b) Behind Back Facing of Wall Panels

Figure 5.12: Temperatures from November 2020 to November 2021

(c) In the Middle of LCC Backfill

Figure 5.12: Temperatures from November 2020 to November 2021 (Continued)

Figure 5.12(a) shows that temperatures at the base of the LCC decreased until May 2021 due to a gradual reduction of the cement hydration rate. From May 2021 to November 2021, temperatures varied slightly with seasonal temperature changes. In addition, the effects from air temperature decreased as the distance from the wall facing increased. From November 2020 to May 2021, low air temperatures decreased LCC temperatures at EPC-03, EPC-04, and EPC-05. EPC-05 was closest to the wall, so it experienced the largest temperature decrease. However, from June 2021 to October 2021, high air temperatures increased LCC temperatures at EPC-03, EPC-04, and EPC-05, with EPC-05 experiencing the largest increase. Furthermore, seasonal temperature changes at the base of the LCC backfill followed seasonal air temperature changes with a time lag. Air temperatures decreased from August 20 to November 5, 2021, but the LCC temperature decrease at EPC-05 began on September 10, 2021.

Figure 5.12(b) shows the effects of cement hydration and air temperature changes on LCC temperatures behind the wall facing. By November 2020 (one month after construction), LCC temperatures directly behind the wall facing were correlated with air temperatures but without daily temperature extremes. As shown in Figure 5.12(c), temperatures in the middle of the LCC decreased with decreasing hydration cement rates and then changed seasonally. In addition, because thermistors T-3 and T-4 were closer to the pavement than thermistors T-1 and T-2, the cooling effect from cold air temperatures from November 2020 to April 2021 caused lower temperatures for T-1 and T-2 than for T-3 and T-4. Similarly, warm air temperatures from May 2021 to November 2021 caused higher temperatures for T-1 and T-2 than for T-3 and T-4. The

effects of air temperature decreased as the distance from the wall facing increased, which could explain the high temperatures for T-2 and T-4 from November 2021 to April 2021 and low temperatures for T-1 and T-3 from May 2021 to November 2021.

Average weekly air temperatures and LCC temperatures were examined long after construction (July 14 to November 5, 2021), as measured by EPC-06 to EPC-10 and the thermistors to eliminate the contribution to LCC temperature from cement hydration. Figure 5.13 shows relationships between these weekly temperatures.

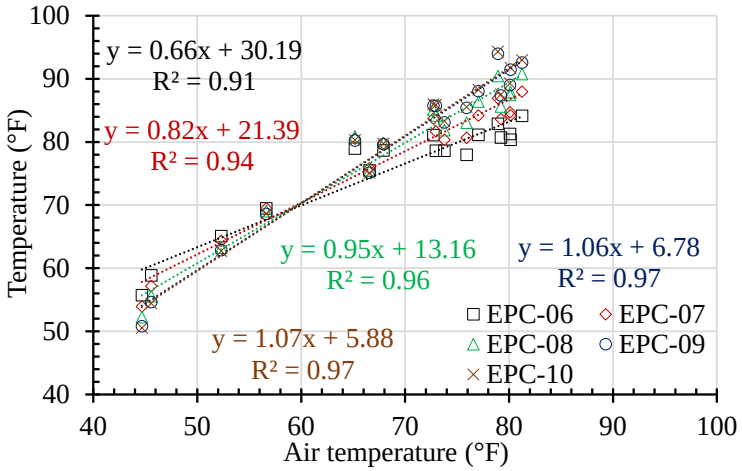

(a) Behind Wall Facing

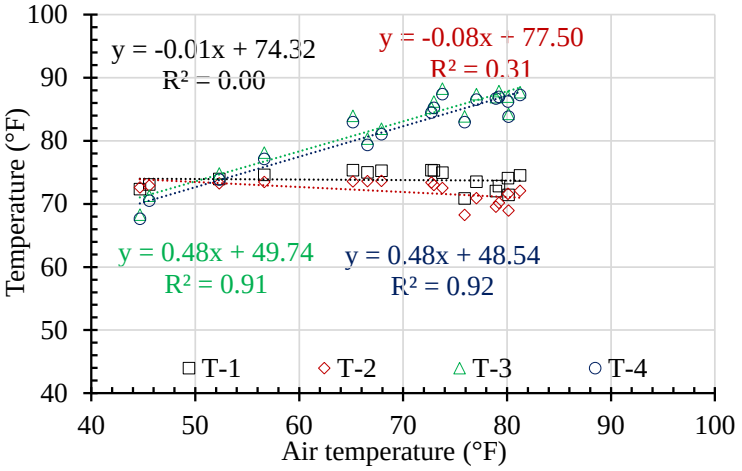

(b) In the Middle of LCC Backfill

Figure 5.13: Relationship between Average Air Temperatures and Average Measured Temperatures

As shown in Figure 5.13, temperatures measured by EPC-06 to EPC-10 and T-3 and T-4 were highly correlated with air temperatures, but the effect of air temperatures on thermistors T-1 and T-2 was minimal. In addition, the temperature response of LCC to air temperature increased from EPC-06 to EPC-10 (increasing slopes in Figure 5.13(a)), as was expected since EPC-06, the lowest pressure cell, was consequently influenced by ground temperatures, and EPC-10, the topmost cell, was most influenced by air temperatures. Furthermore, while T-3, T-4, and EPC-09 were at approximately the same elevation, the slopes for T-3 and T-4 (Figure 5.13(b)) were much smaller than the slope for EPC-09 (Figure 5.13(a)), as was consistent with the deep embedment in the LCC of T-3 and T-4 compared to EPC-09.

5.4 Conclusions

Based on analysis of one-year data from November 1, 2020, to November 5, 2021, more than four months were required for LCC to cool down due to cement hydration. Without consideration of heat due to cement hydration, temperatures behind the wall facing were more readily affected by air temperature than temperatures at the base of the LCC. Following construction of the LCC-MSE wall and LCC curing, vertical earth pressures near the wall facing tended to increase, while vertical earth pressures far from the wall facing tended to decrease over time. Lateral earth pressures behind the wall facing varied daily with daily air temperature variations, meaning lateral earth pressures behind the wall facing should be considered during LCC-MSE wall design since lateral earth pressures behind the wall facing may be greater than expected due to air temperature changes. After opening to traffic, the LCC far from the wall facing demonstrated more significant settling than the LCC near the wall facing. Since the shoulder with less traffic volume was near the wall facing, the settlement difference of LCC may be caused by traffic volume difference. In this study, however, the settlement of ground soil under the LCC-MSE wall induced by LCC weight and traffic loading was less than 0.3 inches.

Chapter 6: Conclusions and Recommendations

As an aggregate alternative backfill material in a mechanically stabilized earth (MSE) wall, lightweight cellular concrete (LCC) has been shown to reduce settlements of ground soil induced by the weight of MSE walls. Although LCC exerts minimal or no lateral earth pressures at the wall facing due to its high strength after curing, temperature-induced stresses are possible. Furthermore, because of the flowability of LCC during placement, no compaction is required during LCC-MSE wall construction, hence eliminating residual lateral earth pressures at the wall facing caused by compaction. In this research, seven steel strips of various lengths were installed during construction of an LCC-MSE wall in Kansas and then pulled out against the wall facing to investigate the pullout capacities of steel strips in LCC. In addition, the LCC-MSE wall was monitored for more than one year after its construction to analyze its performance during construction, LCC curing, and after opening to traffic.

6.1 Conclusions

Research results showed that settlement of the ground soil under the weight of the LCC-MSE wall and traffic loading was less than 0.3 inches, which was less than the adjacent MSE wall with aggregate backfill. Although little to no lateral creep of the wall was observed after the wall had set, there was some lateral movement of the panels during LCC placement. This movement could likely be avoided with more rigid bracing of the panels. Test strip pullout resistances were very consistent among the tests and were much higher than the expected resistance from aggregate backfill with an equivalent overburden pressure. Test strips demonstrated substantial residual pullout resistance even at high deformations.

Regarding temperatures, study results showed that fill temperatures were very high during curing (>200 °F at times), but no negative effects of these high temperatures were observed during curing other than the loss of some sensors. The effect of air temperature changes on lateral earth pressures at the wall facing were much more significant than EPCs at the base of the LCC. High air temperatures were correlated to large lateral pressures at the top of the wall facing. The system may have been rigid enough to cause thermal stresses to develop when significant temperature changes occurred.

During the first 14 days after casting, LCC expansion due to heat emitted from cement hydration appeared to be related to the pullout capacity of the steel strips in the LCC. As temperature decreased, normal stress on the strips caused by LCC expansion decreased, thereby reducing pullout capacity of the strip. From day 14 to day 31 after LCC casting, interface strength gains due to cement hydration counteracted normal strength reduction due to temperature decrease, meaning the pullout capacity remained approximately constant. Results showed that cement hydration increased the pullout capacity of the steel strips in the LCC during the first six months after construction. Because high normal stress on steel strips due to high temperatures was released during the initial pullout test, more time between the initial pullout test and the repull test caused interface strength gains, thus increasing pullout capacity of the repull tests. The pullout capacity of the steel strips did not increase linearly with strip length, which may be caused by differential movements of the long strip along its length.

In addition, during LCC placement, flowable LCC exerted hydraulic pressures on the facing of the LCC-MSE wall, and then pressures on wall panels increased due to the high strength of the LCC and high temperatures caused by cement hydration. Within 12–16 hours after LCC placement, LCC temperatures reached their peak values, meaning the cement hydration rate decreased 12–16 hours after LCC placement. Following construction of the LCC-MSE wall and LCC curing, vertical earth pressures near the wall facing increased, while vertical earth pressures far from the wall facing decreased over time.

6.2 Recommendations

Observations made from this study resulted in several recommendations. First, because LCC was shown to effectively decrease the weight on foundation soils, it should be considered as an alternative to conventional fills where settlement is a concern. Second, high fluid pressures during fill placement require rigid bracing to prevent shifting or tilting of panels during placement of fill. Third, lateral earth pressures at the wall facing in an LCC-MSE wall changed with air temperatures, and high air temperatures may result in higher lateral earth pressures in the upper portion of backfill in LCC-MSE walls compared to AG-MSE walls. A thin layer of expanded polystyrene is recommended for the back of the panels prior to LCC placement to relieve potential

thermal stresses, although additional research is recommended to increase understanding of the issue of earth pressure changes due to air temperature changes. Finally, heat emitted from cement hydration in LCC caused high temperatures in the LCC, which likely damaged installed sensors such as strain gauges. Therefore, the temperature resistance of sensors, or other inclusions such as plastic pipe, should be considered during the design of LCC-MSE walls.

References

AASHTO. (2012). *AASHTO LRFD bridge design specifications* (6th ed.). American Association of State Highway and Transportation Officials.

Berg, R. R., Christopher, B. R., & Samtani, N. C. (2009). *Design of Mechanically Stabilized Earth Walls and Reinforced Soil Slopes – Vol. 1 (FHWA-NHI-10-024).* Federal Highway Administration.

Campbell Scientific. (2017). Instruction manual for 4WFBS120, 4WFBS350, 4WFBS1K 4-wire full-bridge terminal input. Campbell Scientific, Inc.

Chang, D. T., Chang, F. C., Yang, G. S., & Yan, C. Y. (2000). *The influence factors study for geogrid pullout test.* In Grips, Clamps, Clamping Techniques, and Strain Measurement for Testing of Geosynthetics. ASTM International. https://doi.org/978-0-8031-5428-5.

Fouad, F. H. (2006). Cellular concrete. In J. F. Lamond & J. H. Pielert (Eds.), *Significance of tests and properties of concrete and concrete-making materials* (pp. 561–569). ASTM International.

GEOKON. (2021). Model 4800 series VW earth pressure cells instruction manual. GEOKON.

Jayawickrama, P. W., Lawson, W. D., Wood, T. A., & Surles, J. G. (2015). Pullout resistance factors for steel MSE reinforcements embedded in gravelly backfill. *Journal of Geotechnical and Geoenvironmental Engineering*, *141*(2), 04014090. https://doi.org/10.1061/(ASCE)GT.1943-5606.0001192

Jayawickrama, P. W., Surles, J. G., Wood, T. A., & Lawson, W. D. (2013). *Pullout resistance of mechanically stabilized reinforcements in backfills typically used in Texas* (Report No. FHWA/TX-13/0-6493-R1, Vol. 1). Texas Department of Transportation.

Liu, H., Robert, R. L., Han, J., Ye, Y., & O'Reilly, M. (2022). Field pullout tests of steel strips in lightweight cellular concrete backfill. *Journal of Geotechnical and Geoenvironmental Engineering*, *148*(5), 06022004. https://doi.org/10.1061/(ASCE)GT.1943-5606.0002797.

Nambiar, E. K., & Ramamurthy, K. (2006). Influence of filler type on the properties of foam concrete. *Cement and Concrete Composites*, *28*(5), 475–480. https://doi.org/10.1016/j.cemconcomp.2005.12.001

Pradel, D., & Tiwari, B. (2015). *The use of MSE walls backfilled with lightweight cellular concrete in soft ground seismic areas*. In Proceedings of the Third International

Conference of Deep Foundations, Vol. 1, pp. 107–114. Mexican Society for Geotechnical Engineering.

Rahmaninezhad, S. M., Han, J., & Kakrasul, J. I. (2018). Stress distribution and pullout responses of extensile and inextensible reinforcement in soil using different normal loading methods. *The Journal of ASTM International*, *42*(6), 1606–1623. https://doi.org/10.1520/GTJ20180102

Ramezani, M., Vilches, J., & Neitzert, T. (2013). Pull-out behavior of galvanized steel strip in foam concrete. *International Journal of Advanced Structural Engineering*, *5*(1), 24–35. https://doi.org/10.1186/2008-6695-5-24

Sayadi, A. A., Vilches, T. J., Neitzert, T. R., & Clifton, G. C. (2016a). Effectiveness of foamed concrete density and locking patterns on bond strength of galvanized strip. *Construction and Building Materials*, *115*, 221–229. https://doi.org/10.1016/j.conbuildmat.2016.04.047

Sayadi, A. A., Vilches, T. J., Neitzert, T. R., & Clifton, G. C. (2016b). Strength of bearing area and locking area of galvanized strips in foamed concrete. *Construction and Building Materials*, *114*, 56–65. https://doi.org/10.1016/j.conbuildmat.2016.03.146

Taylor, S. M., & Halsted, G. E. (2021). *Guide to lightweight cellular concrete for geotechnical applications* (Report No. PCA Special Report SR1008P). Portland Cement Association and National Concrete Pavement Technology Center at Iowa State University.

Tiwari, B., Ajmera, B., Maw, R., Cole, R., Villegas, D., & Palmerson, P. (2017). Mechanical properties of lightweight cellular concrete for geotechnical applications. *Journal of Materials in Civil Engineering*, *29*(7), 06017007. https://doi.org/10.1061/(ASCE)MT.1943-5533.0001885

Weldu, M. T., Han, J., Rahmaninezhad, S. M., Parsons, R. L., Kakrasul, J.I., & Jiang, Y. (2016). Effect of aggregate uniformity on pullout resistance of steel strip reinforcement. *Transportation Research Record*, *2579*(1), 1–7. https://doi.org/10.3141/2579-01

Ye, Y., Han, J., Liu, H., Rachford, S. M., Parsons, R. L., Dolton, B., & O'Reilly, M. (2022). Pullout resistance of geogrid and steel reinforcement embedded in lightweight cellular concrete backfill. *Geotextile and Geomembrane* (Manuscript in preparation). https://doi.org/10.1016/j.geotexmem.2022.01.001

AD ASTRA PER ASPERA

Kansas

Department of Transportation